The thermal impedance integral and the pathway decomposition of supercritical turbulent heat transfer. Part I. Framework

Ivan Otić*
Institute for Thermal Energy Technology and Safety
Karlsruhe Institute of Technology
Eggenstein-Leopoldshafen, Germany

Özgür Ertunç
Fluid Dynamics and Spray Laboratory
Mechanical Engineering, Özyeğin University
İstanbul, Türkiye

Abstract

The generalised Lyon integral, derived here from the Favre-averaged energy equation without the classical weak-property assumptions, yields three results for turbulent heat transfer to fluids at supercritical pressure. First, the Prandtl and density correction ratios of conventional Nusselt correlations are traced to the molecular and turbulent parts of the integrand, while the integrated specific-heat ratio arises outside the integral, in the enthalpy-to-temperature conversion, and is an eliminable artefact; ten classical correlations map onto this classification, and entanglement of the artefact with the Prandtl correction through the modified Prandtl number produces spurious behaviour near the pseudocritical point. Second, the radial sweep of the pseudocritical barrier through the boundary layer resets the equilibrium underlying the fully developed $\mathrm{Re}/\ln \mathrm{Re}$ scaling, replacing it with the penetration-depth scaling $\mathrm{Nu} \sim \sqrt{\mathrm{Re}}$ in the barrier-dominated regime. Third, separating the integral at the barrier yields wall-side and bulk-side pathways, each characterised by its own thermodynamic state; a two-point quadrature gives a linearised pathway correlation depending only on the bulk Reynolds and Prandtl numbers and a bounded wall-to-bulk Prandtl-number ratio, smooth across the pseudocritical transition and carrying no fitted parameter. These results follow from a single transition: the constant-property Lyon integral, a thermal resistance, becomes a thermal impedance, distinguished by capacitive storage at the specific-heat peak, history dependence through the moving barrier, and response lag of the perpetually developing thermal profile. Experimental validation is provided in the companion paper.

Keywords: supercritical pressure; turbulent heat transfer; variable properties; Nusselt correlation; pseudocritical; thermal resistance

*Corresponding author: ivan.otic@kit.edu

Nomenclature

Roman symbols

a	thermal diffusivity, $\lambda/(\rho c_p)$ [$\mathrm{m^2\,s^{-1}}$]
C	correlation prefactor [–]
c_p	isobaric specific heat [$\mathrm{J\,kg^{-1}\,K^{-1}}$]
$\bar{c}_p$	integrated mean specific heat, $(\tilde{h}_w - \tilde{h}_b)/(T_w - T_b)$ [$\mathrm{J\,kg^{-1}\,K^{-1}}$]
d	pipe inner diameter [m]
f	Darcy friction factor [–]
G	mass flux [$\mathrm{kg\,m^{-2}\,s^{-1}}$]
$g(\mathrm{Pr})$	pathway conductance function [–]
h	specific enthalpy [$\mathrm{J\,kg^{-1}}$]
L	heated length [m]
Nu	Nusselt number [–]
Pr	Prandtl number [–]
$\overline{\mathrm{Pr}}$	modified Prandtl number, $\bar{c}_p\mu/\lambda$ [–]
Pr_t	turbulent Prandtl number [–]
p, q, r	exponents of the property-ratio corrections [–]
q_w	wall heat flux [$\mathrm{W\,m^{-2}}$]
R	pipe radius [m]
Re	Reynolds number [–]
Re_τ	friction Reynolds number [–]
r	radial coordinate [m]
T	temperature [K]
T_{pc}	pseudocritical temperature [K]
u	axial velocity [$\mathrm{m\,s^{-1}}$]
u_τ	friction velocity [$\mathrm{m\,s^{-1}}$]
w	pathway weight [–]
x	axial coordinate [m]
y	wall-normal distance [m]; $y^+ = y\,u_\tau/\nu$
Z	thermal impedance [$\mathrm{K\,m^2\,W^{-1}}$]

Greek symbols

α	heat transfer coefficient [$\mathrm{W\,m^{-2}\,K^{-1}}$]
β	resistance exponent of the pathway conductance [–]
Γ	effective enthalpy transport coefficient [$\mathrm{kg\,m^{-1}\,s^{-1}}$]
δ_{pen}	penetration depth [m]
ε_h, ε_m	eddy diffusivities of heat and momentum [$\mathrm{m^2\,s^{-1}}$]
η	turbulent-to-molecular transport ratio [–]
θ_{pc}	barrier position, $(T_{pc} - T_b)/(T_w - T_b)$ [–]
κ	von Kármán constant [–]
λ	thermal conductivity [$\mathrm{W\,m^{-1}\,K^{-1}}$]
μ	dynamic viscosity [Pa s]
ν	kinematic viscosity [$\mathrm{m^2\,s^{-1}}$]
ξ	logarithmic Prandtl ratio, $\ln(\mathrm{Pr}_b/\mathrm{Pr}_w)$ [–]
ρ	density [$\mathrm{kg\,m^{-3}}$]
ϕ	normalised cumulative mass-flux function [–]

Subscripts and accents

b, w	bulk, wall
pc	pseudocritical
mol, turb, eff	molecular, turbulent, effective
$\bar{\cdot}$, $\tilde{\cdot}$	Reynolds average, Favre average

Abbreviations

DB	Dittus–Boelter correlation
LinP	linearised pathway form
HTD	heat transfer deterioration
TFD	thermally fully developed
Q-mode, T-mode	prediction from heat flux / from measured wall temperature

1 Introduction

1.1 The problem

For constant fluid properties, the Nusselt number for forced convection in a pipe depends only on the Reynolds and Prandtl numbers, both evaluated at a single reference temperature. When properties vary between the wall and the bulk, as they inevitably do under high heat loads or near the critical point, additional multiplicative property-ratio correction factors are introduced in the correlation. Over the past six decades, these factors have been proposed, refined, debated, and accumulated into a substantial body of semi-empirical work: the survey of Vasic et al. [1] lists 194 correlations for heat transfer to fluids at supercritical pressure alone (see also the reviews by Pioro et al. [2], Yoo [3]). The correction factors are commonly constructed via the Buckingham Π-theorem – a dimensional, not a physical, construction – and their physical status has remained largely empirical [2–8].

In engineering practice, one-dimensional system codes such as RELAP5 [9] or APROS [10] are used in the design and safety analysis of supercritical power cycles, for example in the recent research and development of the small modular supercritical-water-cooled reactor (SM-SCWR) within the European–Canadian–Chinese joint project ECC-SMART [11–15]. These codes rely on Nusselt correlations to predict wall temperatures. Near the pseudocritical temperature T_{pc}, the temperature at which isobaric specific heat c_p reaches its maximum at a given supercritical pressure, density, viscosity, thermal conductivity, and specific heat can vary by up to an order of magnitude within temperature intervals of 10–20 K. Figure 1a illustrates this for the Prandtl number of water, evaluated using the CoolProp database [16]. In this range, the choice and form of the correction factors control uncertainty in the wall temperature prediction.

Four structural problems are inherent in the way correlations are constructed and used.

(1) The circularity problem. When a correlation contains wall-evaluated properties such as the wall Prandtl number Pr_w or wall density ρ_w, as nearly all do, the wall temperature T_w appears on both sides of the prediction:

$$T_w \longrightarrow \mathrm{Pr}_w(T_w),\ \rho_w(T_w) \longrightarrow \mathrm{Nu} \longrightarrow T_w. \tag{1}$$

The wall-anchored correlation of Swenson et al. [17], whose Prandtl and density factors are both evaluated at the wall, is a representative case. Away from T_{pc} this iteration may converge stably. However, near the pseudocritical point the extreme sensitivity of wall specific heat capacity $c_{p,w}$, ρ_w and Pr_w to small changes in T_w produces oscillatory or slowly converging iterations. This

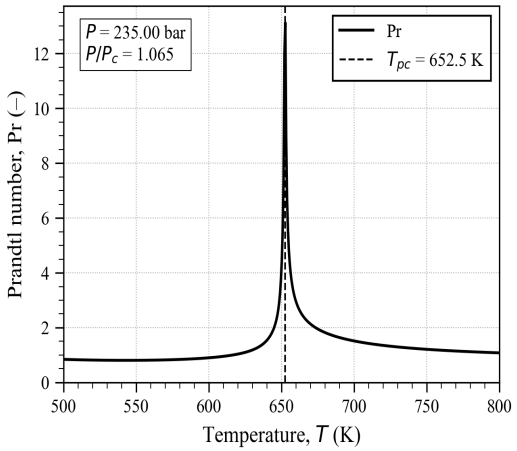

(a) Prandtl number of water at 23.5 MPa as a function of temperature

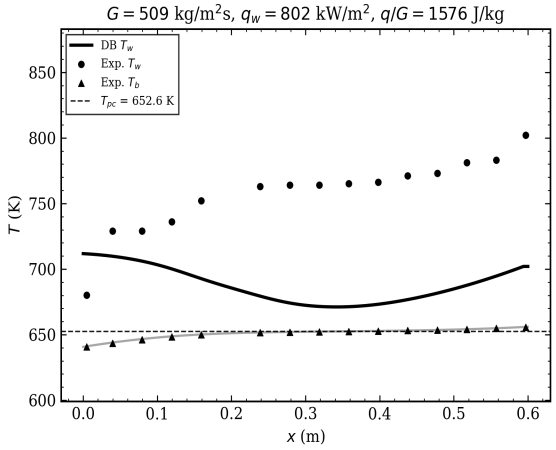

(b) Predicted and experimental results for wall and fluid temperatures along a heated pipe for water at 23.5 MPa (downflow case #104).

amplification is elementary and generic to any wall-evaluated property. For $\mathrm{Nu}_w \propto \mathrm{Pr}_w^n$ $(0 < n < 1)$, the heat transfer coefficient obeys $\alpha \propto \mathrm{Pr}_w(T_b + \Delta T)^n$, where T_b denotes the mass-averaged bulk temperature, and the flux balance $q_w = \alpha\,\Delta T$ yields the circularity gain

$$\frac{\mathrm{d}\ln \Delta T}{\mathrm{d}\ln q_w} = \frac{1}{1 + n\gamma\,\Delta T/T_w}, \qquad \gamma \equiv \frac{\mathrm{d}\ln \mathrm{Pr}_w}{\mathrm{d}\ln T_w}, \tag{2}$$

close to unity far away from T_{pc} but departing sharply where $|\gamma|$ is large, whereupon the iteration oscillates or fails to converge. This feedback (1) is irreducible while any wall property is retained. The integrated-specific-heat factor $(\bar{c}_p/c_{p,b})^n$ superimposes a second amplification: since $\bar{c}_p = \Delta h/\Delta T$, it carries ΔT^{-n} explicitly, giving, to leading order when the enthalpy rise is dominated by the pseudocritical peak, the gain $\mathrm{d}\ln \Delta T/\mathrm{d}\ln q_w = 1/(1-n) > 1$. The factor later shown to be an eliminable artefact (§ 3.1) is thus aggravating, not originating: removing it lowers the gain but does not break the loop, whose root is the wall-property dependence $\mathrm{Nu}(T_w, T_b)$.

The problem is of increasing severity with increasing number of correction factors, creating a fundamental tension between physical accuracy and numerical robustness. This tension is sharpened by the distinction between the *T-method*, in which experimental T_w values are used directly to evaluate properties and assess correlation accuracy, and the *Q-method*, in which the correlation must predict T_w iteratively from a specified heat and mass flux[1]. The Q-method is the mode in which the engineering system codes operate. Correlations that perform well under the T-method can fail under the Q-method, and not only near T_{pc}. More fundamentally, circularity is not a deficiency of any particular correlation but a structural property of the Nusselt number framework itself: any formulation that predicts T_w from $\mathrm{Nu}(T_w)$ necessarily creates a feedback loop whose conditioning deteriorates where properties are most sensitive to temperature.

(2) The spatial mismatch problem. In a heated pipe, for example, the wall and bulk temperatures can traverse the pseudocritical region at different axial positions. Upstream, where $T_w \approx T_{pc}$ but T_b is still well below it, the wall region experiences heat transfer deterioration (HTD) driven by the pseudocritical property transition, while the bulk Prandtl number Pr_b remains stable and Nusselt correlations based on bulk properties are blind to deterioration. Downstream, when T_b

[1] We adopt the terminology of the T- and Q-method introduced by [18–20].

approaches T_{pc} while T_w is already well beyond it, Pr_b spikes sharply, and Dittus–Boelter (DB)-type correlations ($\mathrm{Nu} \propto \mathrm{Pr}_b^{0.4}$) predict a significant increase in heat transfer, even though the wall is in a thermodynamically stable region essentially unaffected by the pseudocritical transition in the bulk. Figure 1b illustrates this case and presents wall and fluid temperature profiles along a heated 0.6 m long pipe ($D = 6.25\,\mathrm{mm}$) at 23.5 MPa, for forced convection in water at mass flux $G = 509\,\mathrm{kg/(m^2\,s)}$ and wall heat flux $q_w = 802\,\mathrm{kW/m^2}$ (downflow case #104, [21, 22]). The T_w profile is computed using the Dittus–Boelter (DB) correlation using the Q-method (numerical approach which is independent of the experimental results and which is described in Section 3 in the companion paper Otić and Ertunç [23]). The DB prediction, anchored to the single bulk state, incurs the spatial mismatch wherever wall and bulk traverse the pseudocritical region at different axial positions (Figure 1b), a defect unavoidable for any correlation built on one thermodynamic state.

(3) The fragmentation problem. The result of six decades of independent work by different groups on different fluids is more than 200 Nusselt correlations (see reviews by [1, 4, 18, 24]), the vast majority of which encode different subsets of correction factors with different exponents, different reference temperatures, and different degrees of entanglement between factors. This fragmentation is itself a symptom of the underlying problem: if the correction factors followed from first principles, the relationships between different architectures would be transparent, and the exponent values would be constrained by theory. Instead, each correlation was commonly fitted independently to a specific experimental dataset processed with a specific set of fluid property tables, and the fitted coefficients absorbed not only the underlying physics but also the systematic errors of those tables. As documented by Kurganov et al. [20], the transition from older property tables [25] to the IAPWS-IF97 standard [26] "disabled practically all commonly used correlations" near T_{pc}, because the empirical coefficients had absorbed the old property-table errors. Re-fitting became necessary, but re-fitting is commonly performed in the less relevant T-mode, compounding the difficulty of distinguishing physics from artefact within the existing correlation structure.

This is a principal reason why classical correlations such as the correlation by [27] are still reported to perform as one of the best when used in Q-mode predictions in engineering system codes, even for supercritical turbulent heat transfer, see e.g. [28–30].

(4) The scaling problem. Beyond the correction-factor mismatch, the experimental data expose a deficiency of existing correlations that has received less attention: the Reynolds-number dependence itself. As the experimental data used in this study show (Section 3.2 in the companion paper Otić and Ertunç [23]), the bulk Reynolds number changes by up to a factor of three between pipe inlet and outlet, driven by the large viscosity decrease as the fluid traverses the pseudocritical region. Under power-plant conditions, this variation can be even stronger. A correlation calibrated at a single Re must implicitly extrapolate across this range within a single pipe, and the fully developed standard exponent $n \approx 0.8$ may no longer be the appropriate scaling in the pseudocritical crossing zone; the constant-property analysis of the Lyon integral [31] shows that even without a pseudocritical crossing the exponent is not a universal constant but drifts with $\ln \mathrm{Re}$.

A closely related difficulty arises from the Prandtl-number dependence. The bulk Prandtl number can change by more than an order of magnitude along the heated length, and in some cases, depending on fluid and boundary conditions, it may decrease downstream of the pseudocritical crossing, whereas in other cases it increases, imposing qualitatively different property trajectories on any single correlation. Many correlations accommodate this variation through a modified Prandtl number $\overline{\mathrm{Pr}}_b = \bar{c}_p\,\mu_b/\lambda_b$, in which the local $c_{p,b}$ is replaced by the integrated mean $\bar{c}_p = (h_w - h_b)/(T_w - T_b)$, where h_w and h_b are wall and bulk enthalpy, respectively. This entangles the intrinsic Prandtl-ratio correction with the eliminable $\bar{c}_p/c_{p,b}$ artefact discussed in Section 3.1, and the entanglement drives spurious behaviour near T_{pc}: the physical sublayer–barrier balance is bounded, whereas $\overline{\mathrm{Pr}}_b$ is not, so a single exponent cannot simultaneously represent both. A pathway decomposition that evalu-

ates each side of the pseudocritical isotherm at its own local Prandtl number, Pr_w and Pr_b, avoids this entanglement by construction (introduced in Section 6).

1.2 Scope and contribution

This paper shows that the property-ratio correction factors, the developing-flow scaling, and the structural limitations of the Nusselt framework all follow from a single transition: the constant-property Lyon integral, which is a thermal *resistance*, becomes a thermal *impedance* when properties vary strongly between wall and bulk. The generalised Lyon integral is derived from the Favre-averaged energy equation without the restrictive assumptions of the classical Petukhov derivation (Section 2.2). Three contributions are established.

(1) The generalised Lyon impedance integral and a unified classification of the correction factors. Based on the derivation for nearly incompressible flows by [32], we derive the generalised Lyon integral (21) for turbulent supercritical flows (Section 2.2). For constant fluid properties, the integral reduces to the classical [33] integral, which is a thermal resistance, a thermal-history-independent quantity evaluated once for a given (Re, Pr) pair. When properties vary strongly, the wall-to-bulk thermal transport develops three features absent from the constant-property case: capacitive thermal storage around the c_p peak in the vicinity of the pseudocritical point, history dependence through the axially sweeping pseudocritical barrier, and response lag of the perpetually developing thermal profile; the generalised Lyon integral that describes it becomes a thermal impedance (Section 3).

Each correction factor in Nusselt correlations arises from a different term in the impedance integrand. The Prandtl ratio $(\mathrm{Pr}_b/\mathrm{Pr}_w)^p$ arises from the balance between the Pr-dependent molecular sublayer and the Pr-independent thermal barrier impedance at the pseudocritical isotherm (Section 3.2). The density ratio $(\rho_w/\rho_b)^r$ arises from the modification of the turbulent diffusivity $\varepsilon_h(r,T)$ through momentum–energy coupling (Section 3.3) and the integrated specific heat ratio $(\bar{c}_p/c_{p,b})^q$ is an artefact of converting enthalpy differences to temperature differences in the global energy balance (Section 3.1). This classification (Table 2) provides a basis to distinguish intrinsic corrections from eliminable ones.

We show in Section 5 that the classical correlations of [34], [35], [36], [37], [38], [24], [27], [17], [39] and [40] all map onto the general structure of Eq. (55) as approximations to the impedance integral under specific assumptions, differing in the choice of reference temperature, the values of the exponents and the degree to which the three corrections are entangled. The analysis reveals that the entanglement of the $\bar{c}_p/c_{p,b}$ artefact with the Prandtl-ratio correction through the modified Prandtl number $\overline{\mathrm{Pr}}_b = \bar{c}_p\,\mu_b/\lambda_b$ is one mechanism responsible for the spurious prediction of heat transfer near the pseudocritical temperature.

(2) The pseudocritical barrier as the source of the impedance character and the developing-flow scaling. When the pseudocritical isotherm lies within the boundary layer, the zone of sharply elevated thermal impedance sweeps radially as the bulk temperature rises along the pipe. At each axial location, the enthalpy shape function inherited from upstream is no longer in equilibrium with the local impedance distribution, and the thermal profile must re-develop from the barrier position outward. This re-development is an internal thermal effect, renewed at every axial location where the barrier position shifts, so that the thermal profile never reaches the fully developed equilibrium underlying the classical $\mathrm{Re}/\ln\mathrm{Re}$ scaling of the constant-property Lyon integral [31] (Section 6.1.3).

The penetration depth of the thermal disturbance growing from the barrier into the turbulent core yields the developing-flow scaling $\mathrm{Nu} \sim \sqrt{\mathrm{Re}}$ (Section 6.1.4), replacing the fully developed exponent $n \approx 0.8$–0.9 with $n = 1/2$ in the barrier-dominated regime. A $1/2$ exponent of this kind, arising when the thermal boundary layer does not reach its fully developed equilibrium, has

precedent in turbulent thermal convection [41–44]; here it emerges for forced flow in a pipe from the continual axial re-development induced by the moving barrier (Section 6.1.4).

For the Dittus–Boelter correlation ($\mathrm{Nu}_b = 0.023\,\mathrm{Re}_b^{0.8}\,\mathrm{Pr}_b^{0.4}$), the prefactor 0.023 is structurally entangled with the $\mathrm{Re}^{0.8}$ scaling and is not simply a consequence of data-based calibration, as established in the companion analysis of the constant-property Lyon integral [31]. Verification against experimental data is presented in Section 2 of the companion paper.

(3) A pathway decomposition of the impedance integral. The thermal barrier regime identified in the impedance integral is approximated by a two-point quadrature that decomposes the boundary layer into wall-side and bulk-side pathways, each characterised by its local Prandtl number (Section 6). In the linearised limit, the pathway decomposition yields a Nusselt form that combines $\sqrt{\mathrm{Re}_b}$, the bulk Prandtl number $\mathrm{Pr}_b^{-\beta}$ with the resistance exponent $\beta = 1/2$, and the bounded ratio $\mathrm{Pr}_b/\mathrm{Pr}_w$ raised to the power $w\beta$, where the symmetric pathway weight $w = 1/2$ follows as the unique unbiased assignment of the two-point quadrature (Eq. (84)). The expression uses only standard Prandtl numbers Pr_b and Pr_w, avoids the artefact $\bar{c}_p/c_{p,b}$, and is smooth across the pseudocritical transition. It serves as the simplest testable consequence of the analysis.

The linearised pathway form is tested in the companion paper [23] against an eighteen-case subset drawn from four experimental databases spanning supercritical water at 23.5–24.5 MPa and CO_2 at 9 MPa, covering Reynolds numbers from 7×10^4 to 2×10^6 and upward, downward and horizontal pipe configurations. The companion paper [23] establishes that the uncalibrated linearised pathway correlation (Eq. (84)) carries the lowest mean Q-mode wall-temperature error across the database, resolves the spatial mismatch problem introduced in §1.1(2) through the symmetric pathway weight $w = 1/2$, and identifies the pathway-resolved ρ_w/ρ_b correction as the missing ingredient required to extend the linearised form to the strongest-contrast supercritical conditions and to the buoyancy-modified downflow regime.

2 The global energy balance and the local thermal impedance

The derivation rests on two exact statements: the global (inlet–outlet) energy balance and the local (wall–bulk) thermal impedance integral. The first relates the wall heat flux to the bulk enthalpy rise; the second determines the heat transfer coefficient at each axial position. We show that every Nusselt correlation is an approximation to the impedance integral under specific assumptions about the property distribution.

2.1 The global energy balance

Consider steady, fully developed turbulent flow through a uniformly heated circular tube of inner diameter d and heated length L. The following is assumed: (1) high Péclet number $\mathrm{Pe} = \mathrm{Re}\cdot\mathrm{Pr} \gg 1$, (2) low Mach number, and (3) no internal heat generation. No assumption on fluid properties is made.

The integral energy balance equates the total wall heat transfer to the bulk enthalpy rise:

$$\dot{Q} = q_w\,\pi d\,L = \dot{m}\,(h_{\mathrm{out}} - h_{\mathrm{in}}) = \dot{m}\,\Delta h, \tag{3}$$

where q_w is the mean wall heat flux, $\dot{m} = \bar{\rho}_b\,\tilde{u}_b\,(\pi d^2/4)$ is the mass flow rate, and $\bar{\rho}_b$ and $\tilde{u}_b$ are the mean bulk density and velocity, respectively. Equation (3) requires no property evaluation at any reference temperature. The wall heat flux is expressed through Newton's law of cooling:

$$q_w = \alpha\,(T_w - T_b), \tag{4}$$

where α is the convective heat transfer coefficient and T_b is the bulk (mass-averaged) temperature. Throughout this paper T_b denotes the mass-averaged bulk temperature. Some correlations (e.g. [35], [36]) use the film temperature $T_f = (T_b + T_w)/2$; where relevant, this is explicitly noted.

2.2 The local wall-to-bulk heat transfer: From thermal resistance to thermal impedance

The classical derivation of the resistance integral is due to [32], who obtained it (his Eqs. 34–41) under three assumptions that are well justified for low property variations but systematically violated near the pseudocritical temperature:

P1. *Weak property fluctuations.* "Physical properties change weakly over the range of temperature fluctuations (i.e., from T to $T + T'$, where T is the averaged temperature value, T' is the temperature fluctuation); therefore, the physical properties at a given point can be considered constant and equal to the physical properties at the averaged temperature", [32].

P2. *Weak density variation.* In particular the density field is assumed to be sufficiently uniform such that Reynolds-averaged and Favre-averaged velocities coincide, $\bar{u} \approx \tilde{u}$, and the density-velocity correlations $\overline{\rho' u'} \approx 0$.

P3. *Local c_p approximation.* The enthalpy gradient can be replaced by $\partial h/\partial r \approx c_p(T)\,\partial T/\partial r$ at every radial position.

Near T_{pc}, all three assumptions fail simultaneously: c_p can change by an order of magnitude within the range of turbulent temperature fluctuations (P1); ρ_w/ρ_b can change almost by an order of magnitude in the small temperature range violating (P2); and the nonlinearity of $h(T)$ and $c_p(T)$ makes P3 inaccurate.

The derivation below shows that the structural form of the impedance integral, and hence the classification of correction factors, does not depend on assumptions P1–P3. By starting from the Favre-averaged enthalpy equation we derive the impedance integral with an effective transport coefficient Γ_{eff} which accounts for the property-fluctuation correlations. Petukhov's classical result is recovered as the limiting case where P1–P3 hold.

The heat transfer coefficient α at each axial position is determined by the local thermal impedance between the wall and the bulk fluid. For variable-density turbulent flow, the appropriate averaging is the mass-weighted, Favre, decomposition:

$$f = \tilde{f} + f'', \qquad \tilde{f} = \frac{\overline{\rho\, f}}{\bar{\rho}}, \tag{5}$$

where $\bar{\cdot}$ denotes the Reynolds time average and $\tilde{\cdot}$ the Favre average. When density variations are weak ($\rho'/\bar{\rho} \ll 1$), $\tilde{f} \approx \bar{f}$, and Favre averaging reduces to Reynolds averaging. Near T_{pc}, where $\rho'/\bar{\rho}$ can be of order unity, the distinction matters.

In the following, $\tilde{u}(r)$ is the Favre-averaged axial velocity, $\tilde{h}(r, x)$ is the Favre-averaged specific enthalpy, $\bar{\rho}(r)$ is the Reynolds-averaged density, and $\bar{T}(r)$ is the Reynolds-averaged temperature. The thermophysical properties λ, c_p, μ are understood to depend on the local temperature $T(r)$ and pressure. The turbulent thermal diffusivity ε_h is written as $\varepsilon_h(r, T)$ to indicate its dependence on both the radial position and the local temperature.

2.2.1 The Favre-averaged energy equation

For steady, axisymmetric, fully developed turbulent flow in a circular tube of radius $R = d/2$, the Favre-averaged energy equation in cylindrical coordinates (r, x), with r measured from the pipe centre, reads:

$$\bar{\rho}\,\tilde{u}(r)\,\frac{\partial \tilde{h}}{\partial x} = \frac{1}{r}\,\frac{\partial}{\partial r}\big[\, r\,\tilde{q}(r)\,\big], \tag{6}$$

where $\tilde{u}(r)$ is the Favre-averaged axial velocity and $\tilde{q}(r)$ is the total (or effective, i.e. molecular plus turbulent) radial heat flux:

$$\tilde{q}(r) = \overline{\lambda\,\frac{\partial T}{\partial r}} \;-\; \bar{\rho}\,\widetilde{u_r''\,h''}. \tag{7}$$

Note that Petukhov's energy equation (his Eq. (1), [32]) is written in Reynolds-averaged form with the molecular conduction approximated as $\bar{\lambda}\,\partial\bar{T}/\partial r$ (assumption P1) and the turbulent flux as $-\rho\,\overline{u_r'\,h'}$ without density weighting (assumption P2).

To integrate (6) we multiply it by $2\pi r\,\mathrm{d}r$ and integrate over the cross section from $r = 0$ to $r = R$

$$2\pi\big[\, r\,\tilde{q}(r)\,\big]_0^R = 2\pi R\,q_w,$$

since $\tilde{q}(0) = 0$ by symmetry and $\tilde{q}(R) = q_w$.

We adopt the assumption that the axial enthalpy gradient is independent of the radius r, which is valid for low-Mach conditions where axial property changes are gradual. It is the only Petukhov assumption (his Eq. (27)) retained in the present derivation and it is physically justified by the fact that the enthalpy shape profile relaxes toward its local equilibrium on an axial length scale much larger than the scale over which the axial property variation changes for the conditions considered here. Therefore,

$$\frac{\partial \tilde{h}}{\partial x}\int_0^R \bar{\rho}\,\tilde{u}\,2\pi r\,\mathrm{d}r = \frac{\partial \tilde{h}}{\partial x}\cdot \pi R^2\,\bar{\rho}_b\,\tilde{u}_b,$$

where the bulk mass-flux velocity is defined by

$$\bar{\rho}_b\,\tilde{u}_b = \frac{2}{R^2}\int_0^R \bar{\rho}(r)\,\tilde{u}(r)\,r\,\mathrm{d}r. \tag{8}$$

Note that this is the Favre-averaged mass flux, not the Reynolds-averaged velocity $\bar{u}_b$; the two differ when $\rho'/\bar{\rho}$ is not negligible. Equating and using $d = 2R$ yields

$$\frac{\partial \tilde{h}}{\partial x} = \frac{4\,q_w}{d\,\bar{\rho}_b\,\tilde{u}_b}. \tag{9}$$

This equation is equivalent to Petukhov's Eq. (29) written in Favre variables; its form is identical because the cross-section integration produces the same mass-flux identity regardless of the averaging.

2.2.2 The radial heat flux profile

Integrate (6) from the centreline to an arbitrary radius r:

$$r\,\tilde{q}(r) = \frac{\partial \tilde{h}}{\partial x}\int_0^r \bar{\rho}(r')\,\tilde{u}(r')\,r'\,\mathrm{d}r'.$$

Substituting (9):

$$\frac{\tilde{q}(r)}{q_w} = \frac{R}{r}\,\phi(r), \tag{10}$$

where the normalised cumulative mass-flux function is

$$\phi(r) = \frac{\displaystyle\int_0^r \bar{\rho}(r')\,\tilde{u}(r')\,r'\,\mathrm{d}r'}{\displaystyle\int_0^R \bar{\rho}(r')\,\tilde{u}(r')\,r'\,\mathrm{d}r'}, \tag{11}$$

satisfying $\phi(0) = 0$ and $\phi(R) = 1$. Note that $\phi(r)$ is defined entirely through the mass flux $\bar{\rho}\,\tilde{u}$ and is independent of c_p.

To obtain the enthalpy profile by integration, we introduce an effective enthalpy transport coefficient $\Gamma_{\text{eff}}(r)$ defined as:

$$\tilde{q}(r) \equiv \Gamma_{\text{eff}}(r)\,\frac{\partial \tilde{h}}{\partial r}. \tag{12}$$

At every radial position where $\partial\tilde{h}/\partial r \neq 0$, Γ_{eff} is uniquely determined by the ratio of the total flux to the enthalpy gradient. As in (7), Γ_{eff} is decomposed as:

$$\Gamma_{\text{eff}}(r) = \underbrace{\Gamma_{\text{mol}}(r)}_{\text{molecular}} + \underbrace{\Gamma_{\text{turb}}(r)}_{\text{turbulent}}, \tag{13}$$

where

$$\Gamma_{\text{mol}}(r) = \frac{\overline{\lambda\,\partial T/\partial r}}{\partial\tilde{h}/\partial r}, \tag{14}$$

$$\Gamma_{\text{turb}}(r) = \frac{-\bar{\rho}\,\widetilde{u_r''\,h''}}{\partial\tilde{h}/\partial r}. \tag{15}$$

The effective coefficient Γ_{eff} accounts for three classes of effects which are neglected in the P1–P3 framework:

(i) *Property-fluctuation correlations* in the molecular term arise when temperature fluctuations T' are large enough that $\lambda(T)$ and $c_p(T)$ vary significantly within the fluctuation range. Near T_{pc}, where c_p has a sharp peak, these correlations can be of order unity relative to the mean terms.

(ii) *Density-velocity correlations* in the turbulent term: the difference between the Favre turbulent flux $\bar{\rho}\,\widetilde{u_r''\,h''}$ and the Reynolds turbulent flux $\bar{\rho}\,\overline{u_r'\,h'}$. These may become significant near T_{pc} where ρ decrease sharply.

(iii) *Turbulent Prandtl number variation* $\mathrm{Pr}_t(r,T)$: the ratio of turbulent momentum to turbulent enthalpy transport, which departs from the standard value ($\mathrm{Pr}_t \approx 0.9$) under strong property gradients. Direct Numerical Simulations (DNS) of supercritical heat transfer in a pipe by Bae et al. [45], with a subsequent assessment of the radial Pr_t distribution by Bae [46], have documented Pr_t variations of order unity in the near-wall region.

Integrating (12) for the enthalpy gradient from any radial position r to the wall yields:

$$\tilde{h}_w - \tilde{h}(r) = \int_r^R \frac{\tilde{q}(r')}{\Gamma_{\text{eff}}(r')}\,\mathrm{d}r'. \tag{16}$$

Substituting the heat flux profile (10) yields

$$\tilde{h}_w - \tilde{h}(r) = q_w\,R \int_r^R \frac{\phi(r')/r'}{\Gamma_{\text{eff}}(r')}\,\mathrm{d}r'. \tag{17}$$

This is the variable-property enthalpy profile. Setting $r = 0$ gives the enthalpy difference between wall and centreline; however, the heat transfer coefficient requires the *bulk* enthalpy, not the centreline value.

The wall-to-bulk enthalpy difference is obtained by mass-flow averaging (17):

$$\tilde{h}_w - \tilde{h}_b = \frac{2}{R^2}\int_0^R \left(\tilde{h}_w - \tilde{h}(r)\right)\frac{\bar{\rho}(r)\,\tilde{u}(r)}{\bar{\rho}_b\,\tilde{u}_b}\,r\,\mathrm{d}r. \tag{18}$$

The squared-integral form (19) is obtained from (18) by substituting the enthalpy profile (17) and exchanging the order of integration. Because this step is central to the structure of the generalised Lyon integral, the intermediate steps are given explicitly in Appendix A.

$$\tilde{h}_w - \tilde{h}_b = q_w\,R \int_0^R \frac{\left[\phi(r)\right]^2}{\Gamma_{\text{eff}}(r)\,r}\,\mathrm{d}r, \qquad \phi(r) = \frac{2}{R^2}\int_0^r \frac{\bar{\rho}(r')\,\tilde{u}(r')}{\bar{\rho}_b\,\tilde{u}_b}\,r'\,\mathrm{d}r'. \tag{19}$$

The physical origin of the squared integral is now transparent. The enthalpy profile (17) contains a factor of the cumulative mass flux (through the heat flux profile $\tilde{q} \propto \phi$), and the mass-flow averaging (18) introduces a second factor of the same cumulative mass flux (through weighting $\bar{\rho}\,\tilde{u}\,r$). The integration-order exchange brings these two factors to the same integration variable, producing the square $[\phi(r)]^2$ in the integrand. This structure, a *squared* mass-flux weighting divided by the local transport coefficient, is the defining feature of the Lyon integral and its generalisations: it ensures that the near-wall region, where both ϕ is large and Γ_{eff} is small, dominates the total impedance.

2.2.3 The generalised Lyon integral

Define the heat transfer coefficient and the integrated specific heat:

$$\alpha = \frac{q_w}{T_w - T_b} = \frac{q_w\,\bar{c}_p}{\tilde{h}_w - \tilde{h}_b}, \qquad \bar{c}_p = \frac{\tilde{h}_w - \tilde{h}_b}{T_w - T_b}. \tag{20}$$

The Nusselt number based on the wall conductivity is $\mathrm{Nu}_w = \alpha\,d/\lambda_w$, so that, with $d = 2R$, $1/\mathrm{Nu}_w = \lambda_w\,(\tilde{h}_w - \tilde{h}_b)/(2\,R\,q_w\,\bar{c}_p)$. Substituting (19):

$$\frac{1}{\mathrm{Nu}_w} = \frac{\lambda_w}{2\,\bar{c}_p}\int_0^R \frac{\left[\phi(r)\right]^2}{\Gamma_{\text{eff}}(r)\,r}\,\mathrm{d}r. \tag{21}$$

This equation is the generalised Lyon integral for variable properties. It has the structural form of Petukhov's Eq. (41). For constant properties, $\bar{\rho}\,\tilde{u}/(\bar{\rho}_b\,\tilde{u}_b)$ reduces to $\bar{u}/\bar{u}_b$, Γ_{eff} becomes uniform, all property ratios become unity, $c_p = \bar{c}_p$, and (21) reduces to the classical Lyon integral ([33]); the reduction is verified against the exact constant-flux limits in Appendix A.

The factor $\bar{c}_p$ in the pre-factor carries the enthalpy–temperature conversion discussed in Section 3.1.

To make the correspondence with Petukhov's Eq. (41) explicit, equation (21) can be written, with $\Gamma_w = \Gamma_{\mathrm{eff}}(R)$ the effective transport coefficient evaluated on the wall, as:

$$\frac{1}{\mathrm{Nu}_w} = \frac{c_{p,w}}{2\,\bar{c}_p} \int_0^R \big[\phi(r)\big]^2 \Big/ \left[\frac{\Gamma_{\mathrm{eff}}(r)}{\Gamma_w}\,\frac{\Gamma_w\,c_{p,w}}{\lambda_w}\,r\right] \mathrm{d}r. \tag{22}$$

In Petukhov's limit, $\Gamma_{\mathrm{eff}}/\Gamma_w = [\lambda\, c_{p,w}/(c_p\,\lambda_w)]\cdot[(1+\frac{\mathrm{Pr}}{\mathrm{Pr}_t}\,\frac{\varepsilon_m}{\nu})/(1+\frac{\mathrm{Pr}_w}{\mathrm{Pr}_t}\,\frac{\varepsilon_{m,w}}{\nu})]$, and the property ratios λ/λ_w and $c_{p,w}/c_p$ from Petukhov's Eq. (41) reappear explicitly. Here ε_m is eddy viscosity; ε_h is eddy diffusivity; and $Pr_t = \varepsilon_m/\varepsilon_h$ is turbulent Prandtl number.

3 The thermal impedance integral

Having derived the generalised Lyon integral (21), we now examine the form it takes when properties vary strongly across the boundary layer. The central result of this section is that the constant-property thermal resistance becomes a thermal impedance, and that this single transition is the common origin of the property-ratio correction factors and the developing-flow scaling derived in the remainder of the paper. The impedance integral has two aspects. Its radial structure, the form of the integrand across the pipe section, determines the property-ratio correction factors and is developed in this section. Its transient character – the capacitive storage, history dependence, and response lag that arise as the pseudocritical barrier sweeps the boundary layer along the pipe – governs the Reynolds-number scaling and is quantified in Section 6.1.4.

For constant fluid properties, the generalised Lyon integral (21) reduces to the classical Lyon integral, in which the integrand depends only on the turbulence structure $\varepsilon_m(r/R)$ and is independent of the temperature field. The resulting quantity $1/\alpha$ is a *thermal resistance* in the strict sense: a thermal-history-independent ratio $\Delta T/q_w$ evaluated once for a given pair (Re, Pr) and applying at every axial position of a fully developed flow.

When properties vary strongly between wall and bulk, and in particular when the pseudocritical isotherm lies within the boundary layer, the integrand of (21) acquires three features absent from the constant-property case that together transform the integral from a resistance into a thermal impedance[2]. These three features are the physical origin of the impedance character and motivate the terminology adopted here. All three are transient in the Lagrangian frame $t = x/\tilde{u}_b$ of a fluid element advected along the pipe; at a fixed axial position the problem remains steady, and the features express themselves as axial structure of the wall-to-bulk transport. Their quantitative consequences are developed in Section 6.1.3 and Section 6.1.4. The correction-factor derivations of Sections 3.1–3.3 depend only on the radial structure of the impedance integrand, independently of these transient features.

Capacitive thermal storage: the sharp c_p peak at T_{pc} creates a narrow zone of very large thermal capacitance per unit volume ($\rho\,c_p$), so that the local heat flux reaching radius r is partly transmitted and partly stored, the partition depending on the rate at which the barrier moves; in the constant-property limit, by contrast, c_p enters only through the Prandtl number as a transport ratio and does not independently affect the total transport. *History dependence:* the enthalpy shape function at axial position x reflects the cumulative effect of the upstream impedance distribution, not merely

[2]The term "impedance" parallels the electrical generalisation of resistance to impedance; see, e.g. Carslaw and Jaeger [47]. Here it denotes a transport quantity that generalises resistance by incorporating reactive thermal capacitance and history-dependent contributions, analogous to the generalisation of electrical resistance when capacitive elements are present. The quantity remains real-valued, with no explicit reactance; the analogy is structural.

Feature	Physical origin	Quantified in
Capacitive storage	c_p peak: flux partly transmitted, partly stored	§ 6.1.3
History dependence	enthalpy profile inherited from upstream	§ 6.1.3
Response lag	perpetually developing profile; $\sqrt{\mathrm{Re}}$ replaces $\mathrm{Re}/\ln \mathrm{Re}$	§ 6.1.4

Table 1: The three features that transform the generalised Lyon integral from a thermal resistance into a thermal impedance.

the local property values – the fully developed assumption of Section 2.2.1 is precisely the condition under which the integral reduces to a memoryless resistance, and the barrier sweep disrupts this equilibrium at every axial position where the barrier position shifts. *Response lag:* the thermal profile is perpetually developing and never reaches the state that would make the response quasi-steady, so the wall temperature at x reflects the impedance distribution over a finite upstream interval; the penetration scaling $\mathrm{Nu} \sim \sqrt{\mathrm{Re}}$ is the quantitative expression of this lag, the turbulent counterpart of the Lévêque–Graetz mechanism [48, 49], driven here by internal re-development at every axial position where the barrier moves rather than by the pipe inlet. Table 1 summarises the three features.

Accordingly, throughout the remainder of this paper the quantity $1/\alpha$ obtained from the variable-property integral (21) is referred to as the *thermal impedance*, and the integral itself as the *thermal impedance integral*. The term *thermal resistance* is reserved for the constant-property limit, for the classical derivations of Petukhov [32] and Lyon [33], where assumptions P1–P3 eliminate the reactive and history-dependent contributions, and for local sub-components of the integral, such as the barrier resistance derived in Section 3.2.3, whose leading-order behaviour is memoryless. The notation Z denotes the thermal impedance throughout.

The derivation of the Nusselt-number correction factors requires equation (21) to be rewritten in impedance form. When the turbulent core is nearly isothermal, so that $\tilde{h}_b \approx \tilde{h}(0)$, the wall-to-bulk enthalpy difference (19) reduces to the wall-to-centreline profile (17) evaluated at $r = 0$; dividing by q_w and converting the enthalpy drop through the local specific heat $c_p\big(T(r)\big)$ yields the thermal impedance

$$Z_{\mathrm{total}} = \int_0^R \frac{R\,\phi(r)/r}{\Gamma_{\mathrm{eff}}(r)\,c_p\big(T(r)\big)}\,\mathrm{d}r, \tag{23}$$

where the local specific heat $c_p(T(r))$ converts the enthalpy-based transport coefficient Γ_{eff}, of units $\mathrm{kg\,m^{-1}\,s^{-1}}$, to the temperature-based effective conductivity. Since $\Gamma_{\mathrm{mol}} = \lambda/c_p$ carries the same local c_p, the conversion is exact,

$$\Gamma_{\mathrm{eff}}(r)\,c_p\big(T(r)\big) = \lambda\big(T(r)\big) + \rho\big(T(r)\big)\,c_p\big(T(r)\big)\,\varepsilon_h(r) \equiv \lambda_{\mathrm{eff}}(r), \tag{24}$$

the local effective thermal conductivity. The quantity Z_{total} carries the units of a thermal impedance, $\mathrm{K\,m^2\,W^{-1}}$, consistent with its role as $\Delta T/q_w$; the wall-unit form used in Section 6.1.1 follows directly. The integrand of (23) has a clear physical meaning: at each radial position, the local heat flux $\tilde{q}(r)$ must be transported across an infinitesimal shell $\mathrm{d}r$ by the combined action of effective molecular and turbulent transport. The total enthalpy drop from wall to bulk is the cumulative effect of these local impedances, weighted by the local heat flux that must pass through each shell. The weighting by $\phi(r)$ ensures that the near-wall region dominates the integral. Two classes of property effects modify this integral, each entering through a different term in the effective transport coefficient:

- *Molecular property variation* (λ, ρ, c_p in Γ_{mol}): origin of the Prandtl-ratio correction (Section 3.2).

- *Turbulent transport modification* (ε_h in Γ_{turb}, modified by density-driven velocity redistribution): origin of the density-ratio correction (Section 3.3).

In general, Γ_{turb} depends on the temperature through the Favre-averaged turbulent enthalpy flux. This temperature dependence arises from two physically distinct mechanisms:

(a) Indirect dependence: density-modified velocity field. When ρ varies across the boundary layer, mass conservation requires redistribution of the velocity field (thermal acceleration, buoyancy), which modifies the mean shear $|\partial\tilde{u}/\partial r|$ and hence the turbulent mixing. This effect is captured by the density-ratio correction $(\rho_w/\rho_b)^r$ derived in Section 3.3.

(b) Direct dependence: turbulent Prandtl number variation and property-fluctuation correlations. The ratio of turbulent momentum to turbulent enthalpy transport, $\mathrm{Pr}_t(r,T)$, departs from its constant-property value under strong property gradients. Additionally, property-fluctuation correlations modify the effective molecular transport. Both effects are absorbed into Γ_{eff} but are *not* captured by any of the three classical correction factors. They are the principal open problem identified in Section 7.

When all properties are independent of temperature, Γ_{eff} reduces to a function of r/R determined solely by the turbulence structure, and the generalised Lyon integral (21) can be evaluated once a turbulence closure $\varepsilon_m(r)$ is specified.

The Lyon integral for constant fluid properties and the resulting Nusselt number scaling are derived in detail in [31], where the Dittus–Boelter correlation (25) is shown to be a power-law representation of the thin-sublayer approximation to the constant-property Lyon integral,

$$\mathrm{Nu}_0 = 0.023\,\mathrm{Re}^{\,0.8}\,\mathrm{Pr}^{\,0.4}, \tag{25}$$

no correction factors are needed because there is only one thermodynamic state.

The central question is: what happens to the generalised Lyon integral (21) and the resulting correlation (25) when the property values at the wall and in the bulk are different?

When T_w and T_b span a region of strong property variation, the energy balance (3) remains exact, but the temperature field cannot be evaluated by evaluating properties at a single reference temperature. This is reflected by the generalised Lyon integral (21) and becomes obvious from the integrand of the impedance form (23). The local thermal impedance $1/[\Gamma_{\text{eff}}(r)\,c_p(T(r))] = 1/\lambda_{\text{eff}}(r)$ varies across the pipe cross section through the temperature field $T(r)$. When the pseudocritical isotherm T_{pc} falls between T_b and T_w, a sharp peak develops at the radial position where $T(r) = T_{pc}$: there λ passes through its steepest decrease and c_p through its maximum, producing a zone of locally high impedance. Additionally, in this region, the property-fluctuation correlations absorbed by Γ_{eff} are at their most intense, further modifying the local transport. This is the mechanism of the spatial mismatch problem introduced in the Introduction.

From the above follows that a single reference-temperature evaluation cannot simultaneously capture:
(i) the near-wall molecular transport (dominated by $\Gamma_{\text{mol},w}$),
(ii) the pseudocritical barrier zone (where both Γ_{mol} and Γ_{turb} change rapidly) and
(iii) the bulk transport (dominated by $\Gamma_{\text{mol},b}$ and $\Gamma_{\text{turb},b}$).
Approximating this structured integral requires at minimum *two* evaluation points: one characterising the near-wall region and one the bulk. Note that this requirement is already implicit in the generalised Lyon integral (21) through the pre-factor $\lambda_w/\bar{c}_p$, which involves both the wall and the wall-to-bulk averaged thermodynamic states.

In terms of correlations, this means that representing the generalised Lyon integral by a power-law correlation of the Dittus–Boelter type (25) requires the property variation to be absorbed into

multiplicative correction factors, formed as ratios of properties evaluated at two reference temperatures. The following three subsections derive these factors from the structure of the generalised Lyon integral and classify them by their origin.

3.1 Correction I: the specific heat ratio $\bar{c}_p/c_{p,b}$ is an artefact

The first correction factor does not arise from the structure of the impedance integral, but from the conversion between the enthalpy-based and temperature-based definitions of the heat-transfer coefficient. It can therefore be isolated before the integral itself is analysed.

The generalised Lyon integral (21) expresses $1/\mathrm{Nu}_w$ in terms of $\tilde{h}_w - \tilde{h}_b$ (through the definition $\alpha = q_w\,\bar{c}_p/(\tilde{h}_w - \tilde{h}_b)$). The resulting pre-factor $c_{p,w}/\bar{c}_p$ of the transparent form (22) involves the integrated specific heat

$$\bar{c}_p \equiv \frac{\tilde{h}_w - \tilde{h}_b}{T_w - T_b} = \frac{1}{T_w - T_b}\int_{T_b}^{T_w} c_p(T)\,\mathrm{d}T. \tag{26}$$

This quantity is not a physical property at any single temperature, it is a conversion factor between Δh and ΔT. If one defines the Nusselt number directly in terms of enthalpy, $\bar{c}_p$ never appears. Crucially, this factor is independent of the averaging convention (Favre or Reynolds) and of the effective transport coefficient Γ_{eff}: it arises purely from the definition of α in (20).

To make the origin of the $\bar{c}_p/c_{p,b}$ factor explicit, we non-dimensionalise the generalised Lyon integral (21) with bulk properties. From the definition $\mathrm{Nu}_b = \alpha\,d/\lambda_b = q_w\,d/[\lambda_b\,(T_w - T_b)]$ using $\alpha = q_w\,\bar{c}_p/(\tilde{h}_w - \tilde{h}_b)$ yields

$$\mathrm{Nu}_b = \frac{\lambda_w}{\lambda_b}\,\frac{\bar{c}_p}{c_{p,w}}\,\frac{1}{\dfrac{\lambda_w}{2\,c_{p,w}}\displaystyle\int_0^R \frac{[\phi(r)]^2}{\Gamma_{\mathrm{eff}}(r)\,r}\,\mathrm{d}r}. \tag{27}$$

Separating the factors that depend on the wall-to-bulk properties from the integral yields

$$\mathrm{Nu}_b = \underbrace{\frac{\bar{c}_p}{c_{p,b}}}_{\substack{\text{enthalpy–temperature}\\ \text{conversion}}} \times \underbrace{\frac{\lambda_w}{\lambda_b}\,\frac{c_{p,b}}{c_{p,w}}}_{\substack{\text{reference-temperature}\\ \text{shift}}} \times \underbrace{\frac{1}{\dfrac{\lambda_w}{2\,c_{p,w}}\displaystyle\int_0^R \frac{[\phi]^2}{\Gamma_{\mathrm{eff}}\,r}\,\mathrm{d}r}}_{\text{impedance integral}}. \tag{28}$$

The first factor, $\bar{c}_p/c_{p,b}$, arises solely because we chose to express the energy balance in terms of ΔT rather than Δh. It is independent of the molecular transport, the turbulent transport, and the property-fluctuation correlations. It is entirely a consequence of global energy-balance bookkeeping when Δh is converted to ΔT.

3.2 Correction II: the Prandtl ratio $\mathrm{Pr}_b/\mathrm{Pr}_w$ from the thermal impedance integral

The Prandtl-ratio correction arises from the variation of the molecular component of the effective transport coefficient, $\Gamma_{\mathrm{mol}}(r)$, across the integrand of the impedance integral (23). In the Reynolds-averaged limit, $\Gamma_{\mathrm{mol}} = \lambda/c_p$ and its variation is controlled by $\lambda(T)$, $\rho(T)$, $c_p(T)$ evaluated at the local mean temperature. In the general framework, Γ_{mol} additionally absorbs the property-fluctuation correlations $\overline{\lambda'\,\partial T'/\partial r}$, but the structural dependence on the local Prandtl number is the same. Unlike the $\bar{c}_p/c_{p,b}$ factor, which is a pre-factor outside the integral, the Prandtl ratio emerges from the integrand itself and is intrinsic to the heat transfer problem.

The derivation below identifies the Prandtl-number dependence directly from the integrand of (23) in three steps: factorisation of the integrand to isolate Γ_{mol}, identification of the molecular-dominated zone and its Pr-dependent extent, and evaluation in the two limiting regimes.

3.2.1 Factorisation of the integrand

(23) and (24) yield

$$Z_{\text{total}} = \int_0^R \frac{R\,\phi(r)/r}{\lambda\big(T(r)\big) + \rho\big(T(r)\big)\,c_p\big(T(r)\big)\,\varepsilon_h(r,T)}\,\mathrm{d}r. \tag{29}$$

The denominator of (29) is the local effective thermal conductivity $\lambda_{\text{eff}}(r) = \Gamma_{\text{eff}}(r)\,c_p(T(r)) = \lambda + \rho\,c_p\,\varepsilon_h$ of (24), in which both the molecular conductivity and the turbulent contribution $\rho\,c_p\,\varepsilon_h$ vary strongly with temperature across the wall–bulk interval; it is this variation that the constant-property derivation suppresses. In order to derive simplified dimensionless correlations from the impedance integral (29) further simplification is required. The thin-sublayer impedance integral assumes $\phi \approx 1$, $r \approx R$ and for the wall-normal coordinate $y = R - r$, reads:

$$Z_{\text{total}} = \int_0^\delta \frac{1}{\lambda\big(T(y)\big) + \rho\big(T(y)\big)\,c_p\big(T(y)\big)\,\varepsilon_h(y,T)}\mathrm{d}y, \tag{30}$$

where δ is an outer limit beyond which the turbulent core is effectively isothermal and contributes negligibly to the impedance. Factoring $\lambda(T)$ out gives

$$Z_{\text{total}} = \int_0^\delta \frac{1}{\lambda\big(T(y)\big)}\,\frac{1}{1+\eta(y,T)}\mathrm{d}y, \tag{31}$$

where

$$\eta(y,T) \equiv \frac{\rho\,c_p\,\varepsilon_h}{\lambda} = \frac{\varepsilon_h(y)}{a(T(y))} = \frac{\varepsilon_h(y)\,\mathrm{Pr}\big(T(y)\big)}{\nu\big(T(y)\big)} \tag{32}$$

is the local ratio of turbulent to molecular transport. Here $a = \lambda/(\rho\,c_p) = \nu/\mathrm{Pr}$ is the local thermal diffusivity. All quantities, including dimensionless ones, are local and temperature and pressure dependent. The factorisation (31) makes explicit that the local Prandtl number enters the impedance integral through two distinct roles:

1. The prefactor $1/\lambda(T)$ sets the molecular impedance scale at each radial position.
2. The transport ratio $\eta \propto \mathrm{Pr}\cdot\varepsilon_h/\nu$ determines where the transition from molecular to turbulent transport occurs, and therefore which radial zone dominates the integral.

3.2.2 The molecular-dominated zone and its Pr-dependent thickness

The integrand in (31) has two asymptotic behaviours:

- For $\eta \ll 1$ (near the wall): the factor $1/(1+\eta) \approx 1$, and the local impedance is $1/\lambda(T)$. Molecular conduction controls the transport.
- For $\eta \gg 1$ (in the turbulent core): the factor $1/(1+\eta) \approx 1/\eta$, and the impedance drops to $\nu/(\varepsilon_h\,\mathrm{Pr})$.

We define the outer edge of this zone, y_c, by the crossover condition $\eta(y_c) = 1$:

$$\varepsilon_h(y_c) = a\big(T(y_c)\big) = \frac{\nu\big(T(y_c)\big)}{\mathrm{Pr}\big(T(y_c)\big)}. \tag{33}$$

The near-wall asymptotic behaviour of the turbulent thermal diffusivity follows the classical cubic law $\varepsilon_h \sim (\nu_w/\mathrm{Pr}_t)\,(y^+)^3$ for $y^+ \to 0$, where $y^+ = y\,u_\tau/\nu_w$ is the wall-normal distance in viscous units and u_τ is the friction velocity, see e.g. Schlichting and Gersten [50]. Substituting into (33) and evaluating the molecular properties at the wall temperature (since $T \approx T_w$ throughout this thin layer):

$$\frac{\nu_w}{\mathrm{Pr}_t}\,(y_c^+)^3 \sim \frac{\nu_w}{\mathrm{Pr}_w}, \qquad \Longrightarrow \qquad y_c^+ \sim \left(\frac{\mathrm{Pr}_t}{\mathrm{Pr}_w}\right)^{1/3}. \tag{34}$$

Therefore, the radial extent of the molecular-dominated zone, and hence the portion of the integrand that samples $1/\lambda$ rather than the turbulent bypass, is set by Pr_w. Higher Pr_w shrinks y_c^+, moving the crossover closer to the wall.

3.2.3 Two regimes of the impedance integral

The behaviour of (31) within the molecular-dominated zone ($0 \le y \le y_c$) depends qualitatively on how $1/\lambda(T)$ varies across that zone. This variation is controlled by whether the pseudocritical isotherm T_{pc} falls within the boundary layer.

Standard regime (T_{pc} outside the boundary layer). When T_{pc} lies outside the range $[T_b,\, T_w]$, properties vary smoothly across the molecular zone. The thermal conductivity is approximately constant at λ_w throughout $y < y_c$, and the impedance integral is controlled by the thickness of the molecular zone:

$$Z_{\mathrm{mol}} = \int_0^{y_c} \frac{1}{\lambda(T(y))}\,\frac{\mathrm{d}y}{1+\eta} \;\approx\; \frac{y_c}{\lambda_w}. \tag{35}$$

Converting to wall units using $y_c = y_c^+\,\nu_w/u_\tau$ and substituting (34):

$$Z_{\mathrm{mol}} \sim \frac{\nu_w}{\lambda_w\,u_\tau}\left(\frac{\mathrm{Pr}_t}{\mathrm{Pr}_w}\right)^{1/3}. \tag{36}$$

To make the Pr_w-dependence explicit, we rewrite the prefactor ν_w/λ_w using the definitions $\mathrm{Pr}_w = \nu_w/a_w = \mu_w c_{p,w}/\lambda_w$ and $a_w = \lambda_w/(\rho_w c_{p,w})$:

$$\frac{\nu_w}{\lambda_w} = \frac{\nu_w}{a_w}\,\frac{a_w}{\lambda_w} = \frac{\mathrm{Pr}_w}{\rho_w\,c_{p,w}}. \tag{37}$$

Substituting (37) into (36) yields:

$$Z_{\mathrm{mol}} \sim \frac{\mathrm{Pr}_w}{\rho_w\,c_{p,w}\,u_\tau}\,\mathrm{Pr}_w^{-1/3}\,\mathrm{Pr}_t^{1/3} = \frac{\mathrm{Pr}_w^{2/3}\,\mathrm{Pr}_t^{1/3}}{\rho_w\,c_{p,w}\,u_\tau}. \tag{38}$$

The corresponding conductance (inverse resistance) is therefore:

$$g_{\mathrm{std}} = Z_{\mathrm{mol}}^{-1} \propto \mathrm{Pr}_w^{-2/3}. \tag{39}$$

Two competing effects produce this scaling. The prefactor $\nu_w/\lambda_w \propto \mathrm{Pr}_w$ means that higher Pr_w increases the molecular impedance at each point within the sublayer. Simultaneously, the sublayer thickness $y_c^+ \propto \mathrm{Pr}_w^{-1/3}$ shrinks, reducing the path length over which that impedance acts. The net

conductance scales as $\mathrm{Pr}_w^{-2/3}$. This is the sublayer-thinning effect: the geometric narrowing of the molecular zone partially, but not fully, compensates for the higher pointwise impedance.

Thermal barrier regime (T_{pc} inside the boundary layer). When T_{pc} falls between T_b and T_w, the factor $1/\lambda\big(T(y)\big)$ in the integrand (31) develops a sharp peak at the radial position y_{pc} where $T(y_{pc}) = T_{pc}$: there λ passes through its steepest decrease and c_p through its maximum. In this regime, the integral is no longer controlled by the geometric thickness y_c of the molecular zone; instead, it is dominated by the peak value of the integrand.

We now show that, in contrast to the standard regime, the barrier resistance is to leading order *independent* of the local Prandtl number, a cancellation that has direct consequences for the form of the Prandtl-ratio correction in the Nusselt correlations.

Consider the impedance integral (31) evaluated over the barrier zone centred on y_{pc}. Within this zone the transport ratio η need not be small: the barrier is not in general confined to the viscous sublayer. The local effective thermal conductivity is $\lambda_{\mathrm{eff}} = \lambda(1+\eta)$, and the integrand takes the form $[\lambda(1+\eta)]^{-1}$.

The temperature gradient within the barrier zone is set by the local energy balance:

$$\frac{\mathrm{d}T}{\mathrm{d}y} \sim \frac{q_w}{\lambda_{\mathrm{eff}}} = \frac{q_w}{\lambda(1+\eta)}. \tag{40}$$

The radial extent of the zone over which properties deviate significantly from their far-field values is set by the temperature interval ΔT_{pc} characterising the c_p peak. From (40), this radial extent is:

$$\Delta y_{pc} \sim \frac{\lambda_{\min}(1+\eta_{pc})\,\Delta T_{pc}}{q_w}, \tag{41}$$

where $\lambda_{\min} \equiv \lambda(T_{pc})$ and $\eta_{pc} \equiv \eta(y_{pc}, T_{pc})$. Note that Δy_{pc} depends on the local transport: both the molecular conductivity $\lambda_{\min}$ and the turbulent bypass factor $(1+\eta_{pc})$ set the radial width.

The barrier resistance is the product of the local impedance and the zone width:

$$Z_{\mathrm{barrier}} = \int_{\mathrm{peak}} \frac{1}{\lambda(1+\eta)}\,\mathrm{d}y \;\sim\; \frac{1}{\lambda_{\min}(1+\eta_{pc})}\,\Delta y_{pc}. \tag{42}$$

Substituting (41):

$$Z_{\mathrm{barrier}} \;\sim\; \frac{1}{\lambda_{\min}(1+\eta_{pc})} \cdot \frac{\lambda_{\min}(1+\eta_{pc})\,\Delta T_{pc}}{q_w} \;=\; \frac{\Delta T_{pc}}{q_w}. \tag{43}$$

The cancellation is exact to leading order: the same effective conductivity $\lambda_{\min}(1+\eta_{pc})$ that determines the pointwise impedance also sets the temperature gradient and hence the radial extent of the barrier zone. The product (impedance $\times$ width) is independent of both the molecular conductivity and the turbulent bypass factor. The physical content of (43) is that ΔT_{pc} is a thermodynamic constant of the fluid at the given pressure, set by the width of the c_p peak and independent of the transport: the barrier resistance is fixed by the fluid state, not by the flow. Crucially, the barrier resistance (43) depends only on the thermodynamic width ΔT_{pc} of the c_p peak and the imposed heat flux q_w; it is, to leading order, independent of Pr.

This cancellation has a precise interpretation within the resistance–impedance distinction introduced above. The thermal impedance of the barrier zone has, in general, both a resistive component (the steady-state transport through the local effective conductivity) and a reactive (capacitive) component (the enthalpy storage associated with the large $\rho\, c_p$ at T_{pc}). In the product (pointwise impedance) $\times$ (zone width) (43), both components scale with $\lambda_{\min}(1+\eta_{pc})$: the resistive part

through the pointwise impedance, the capacitive part through the temperature gradient that sets the zone width. The product therefore cancels to $\Delta T_{pc}/q_w$, a thermal-history-independent quantity, that is, a pure *resistance*. The barrier zone, taken in isolation, is memoryless to leading order. The impedance character of the total wall-to-bulk transport arises not from the barrier itself but from its interaction with the rest of the boundary layer: the barrier sweeps radially as T_b rises, continuously resetting the thermal profile on either side (discussed in detail later in the Section 6.1.3), so that the upstream thermal history enters the integral at every axial position. The local resistance of the barrier and the global impedance of the wall-to-bulk path are therefore distinct quantities, and the Pr-independence of (43) is a property of the former, not the latter.

This cancellation holds as long as η is approximately constant across the narrow barrier zone. Near T_{pc}, where Pr has a sharp peak, η itself varies rapidly across the barrier, introducing higher-order Pr-dependent corrections. These corrections are absorbed into the empirical exponent p in the power-law parameterisation derived below, but the leading-order Pr-independence remains.

Origin of the Prandtl-ratio correction from the impedance balance.

The Prandtl-ratio correction factor arises not from the barrier resistance itself (which is Pr-independent to leading order) but from the balance between the barrier resistance and the Pr-dependent sublayer resistance.

The total impedance between wall and bulk is the sum of the sublayer contribution and the barrier contribution:

$$Z_{\text{total}} = Z_{\text{sublayer}} + Z_{\text{barrier}}. \tag{44}$$

From (38), the sublayer resistance scales as $Z_{\text{sublayer}} \propto \text{Pr}_w^{2/3}$. From (43), the barrier resistance is $Z_{\text{barrier}} \sim \Delta T_{pc}/q_w$, independent of Pr to leading order.

The constant-property reference resistance, evaluated at bulk conditions, scales as $Z_0 \propto \text{Pr}_b^{2/3}$. The Nusselt number ratio is therefore:

$$\frac{\text{Nu}}{\text{Nu}_0} = \frac{Z_0}{Z_{\text{total}}} = \frac{A\,\text{Pr}_b^{2/3}}{B\,\text{Pr}_w^{2/3} + Z_{\text{barrier}}}, \tag{45}$$

where A and B contain the non-Pr prefactors.

Limit 1: No barrier ($Z_{\text{barrier}} \ll Z_{\text{sublayer}}$).

$$\frac{\text{Nu}}{\text{Nu}_0} \approx \frac{A}{B}\left(\frac{\text{Pr}_b}{\text{Pr}_w}\right)^{2/3}. \tag{46}$$

Limit 2: Barrier-dominated ($Z_{\text{barrier}} \gg Z_{\text{sublayer}}$).

$$\frac{\text{Nu}}{\text{Nu}_0} \approx \frac{A\,\text{Pr}_b^{2/3}}{Z_{\text{barrier}}}, \tag{47}$$

which is independent of Pr_w.

In the intermediate regime, the power-law parameterisation

$$\frac{\text{Nu}}{\text{Nu}_0} \approx \left(\frac{\text{Pr}_b}{\text{Pr}_w}\right)^p, \qquad 0 < p < \tfrac{2}{3}, \tag{48}$$

approximates (45) with an effective exponent p that encodes the fractional importance of the barrier.

The direction of the Prandtl ratio, $(\text{Pr}_b/\text{Pr}_w)^p$ with $p > 0$, is uniquely determined by the physics of the impedance integral. When $\text{Pr}_w > \text{Pr}_b$, the near-wall molecular impedance exceeds the baseline; the Nusselt number must be *reduced*. Therefore,

$$\frac{\text{Nu}}{\text{Nu}_0} = \mathcal{G}(\text{Pr}_w, \text{Pr}_b) \approx \left(\frac{\text{Pr}_b}{\text{Pr}_w}\right)^p, \tag{49}$$

where $p > 0$ captures the net effect of the property variation across the integrand. The formulation of $\mathcal{G}$ is inconsistent in the literature, sometimes introducing entanglement that induces prediction errors in the Q-mode. This is discussed in detail in Section 4.

3.3 Correction III: the density ratio ρ_w/ρ_b from momentum–energy coupling

The density-ratio correction enters the impedance integral through a different factor in the integrand than the Prandtl-ratio correction. Recall the factored form (31):

$$Z_{\text{total}} = \int_0^{\delta} \underbrace{\frac{1}{\lambda\big(T(y)\big)}}_{\text{molecular impedance}} \cdot \underbrace{\frac{\mathrm{d}y}{1+\eta(y,T)}}_{\text{turbulent bypass}}, \tag{50}$$

The two corrections are structurally distinct in the integrand: one acts on the molecular impedance, the other on the turbulent bypass efficiency. When the two factors are perturbed independently about their constant-property values a_0, b_0,

$$Z = \int a\, b\, \mathrm{d}y \;\approx\; \left(\int a\, b_0\, \mathrm{d}y\right) \cdot \frac{\displaystyle\int a_0\, b\, \mathrm{d}y}{\displaystyle\int a_0\, b_0\, \mathrm{d}y}, \tag{51}$$

which factorises into the product of two independent corrections, provided the mixed perturbation $\int \delta a\, \delta b\, \mathrm{d}y$ is small. This condition is well satisfied when the property variation is moderate. Near T_{pc}, however, both perturbations are simultaneously large and spatially correlated, and the multiplicative independence degrades.

When $\rho_w \neq \rho_b$, mass conservation requires velocity redistribution (thermal acceleration, buoyancy), which modifies the mean shear $|\partial\tilde{u}/\partial r|$ and modifies the transport ratio $\eta(y)$. In the mixing-length framework, the turbulent thermal diffusivity scales with the mean shear as:

$$\varepsilon_h(y) \sim \frac{\ell^2\, |\partial\tilde{u}/\partial y|}{\mathrm{Pr}_t}. \tag{52}$$

The density-modified turbulent diffusivity is parameterised as:

$$\varepsilon_{h,\text{eff}}(y) \sim \varepsilon_{h,0}(y) \cdot \mathcal{F}\left(y,\, \frac{\rho_w}{\rho_b}\right). \tag{53}$$

Since the density modification enters the integral multiplicatively through η, parameterising the functional $\mathcal{F}$ in power-law form:

$$\frac{\mathrm{Nu}}{\mathrm{Nu}_0} \propto \left(\frac{\rho_w}{\rho_b}\right)^r, \tag{54}$$

where the exponent r absorbs both the radial structure of $\mathcal{F}$ and the flow-configuration dependence. The quantitative prediction of r from first principles requires solving the coupled momentum–energy problem; this is deferred to a separate study.

Factor	Exponent	Component of Γ_{eff}	Origin
$C\,\mathrm{Re}_b^n\,\mathrm{Pr}_b^m$	$n,\ m$	entire Γ_{eff} (uniform)	constant-property Lyon integral
$(\mathrm{Pr}_b/\mathrm{Pr}_w)^p$	$p \in (0, 2/3)$	Γ_{mol}	sublayer–barrier resistance balance
$(\bar{c}_p/c_{p,b})^q$	$q \approx 0.4$–0.7	none (pre-factor)	$\Delta h \leftrightarrow \Delta T$ conversion
$(\rho_w/\rho_b)^r$	$r \approx 0.3$–0.4	Γ_{turb}	density-driven velocity redistribution
(unresolved)	—	$\Gamma_{\text{eff}} - \Gamma_{\text{Petukhov}}$	property-fluctuation correlations, $\mathrm{Pr}_t(r,T)$ variation, Pr–ρ cross-coupling near T_{pc}

Table 2: Origin and classification of the correction factors by their role in the generalised Lyon integral (21) and the effective transport coefficient Γ_{eff} (Eq. (13)).

4 The general correlation structure

Combining the results of Sections 3.1–3.3, the variable-property Nusselt number takes the form:

$$\mathrm{Nu}_b = C\,\mathrm{Re}_b^n\,\mathrm{Pr}_b^m \underbrace{\left(\frac{\mathrm{Pr}_b}{\mathrm{Pr}_w}\right)^p}_{\substack{\text{sublayer–barrier}\\ \text{balance}\\ (\Gamma_{\text{mol}}\text{ in integrand})}} \cdot \underbrace{\left(\frac{\bar{c}_p}{c_{p,b}}\right)^q}_{\substack{\text{enthalpy–temperature}\\ \text{conversion}\\ \text{(pre-factor)}}} \cdot \underbrace{\left(\frac{\rho_w}{\rho_b}\right)^r}_{\substack{\text{momentum–energy}\\ \text{coupling}\\ (\Gamma_{\text{turb}}\text{ in integrand})}} \tag{55}$$

Each factor is now traced to a specific component of the generalised Lyon integral (21) and the effective transport coefficient decomposition $\Gamma_{\text{eff}} = \Gamma_{\text{mol}} + \Gamma_{\text{turb}}$:

- The baseline $C\,\mathrm{Re}_b^n\,\mathrm{Pr}_b^m$ represents the constant-property Lyon integral, where Γ_{eff} is uniform and the impedance scales as $\mathrm{Pr}_b^{2/3}$.
- The Prandtl ratio $(\mathrm{Pr}_b/\mathrm{Pr}_w)^p$ captures the balance between the Pr_w-dependent sublayer resistance and the Pr-independent barrier resistance. The exponent p encodes the fractional importance of the barrier: $p \to 2/3$ when the barrier is negligible, $p \to 0$ when the barrier dominates.
- The specific heat ratio $(\bar{c}_p/c_{p,b})^q$ is the pre-factor from the enthalpy-to-temperature conversion. It is external to Γ_{eff} entirely and eliminable: in an enthalpy-based formulation, $q = 0$.
- The density ratio $(\rho_w/\rho_b)^r$ captures the modification of Γ_{turb} through density-driven velocity redistribution.

Of the three correction factors, only the $\bar{c}_p/c_{p,b}$ ratio is fully resolved by the present analysis: it is an artefact, eliminable by reformulation. The Prandtl ratio and density ratio are intrinsic, and their origins in the impedance integral are established, but the exponents still require empirical or computational input.

The contribution of the framework is not to eliminate empiricism but to confine it to physically meaningful parameters and to identify the regime where each correction is active: p is bounded by the sublayer–barrier balance ($0 < p < 2/3$), and r is set by the momentum–energy coupling strength. Each factor is now traced to a specific component of the generalised Lyon integral (21) and the effective transport coefficient decomposition $\Gamma_{\text{eff}} = \Gamma_{\text{mol}} + \Gamma_{\text{turb}}$, as summarised in Table 2.

What the framework does not capture The property-fluctuation correlations and turbulent Prandtl number variation absorbed by Γ_{eff} do not map cleanly onto any of the three classical correction factors. Additionally, the multiplicative independence of the Prandtl and density corrections

degrades near T_{pc}, where both perturbations are simultaneously large. Resolving these effects, e.g. through DNS-based parameterisations of $\mathrm{Pr}_t(r, T)$, is an open problem identified in Section 7.

The principal physical limitation is the fully developed flow assumption, which is violated at higher heat loads and under supercritical conditions, as discussed in Section 1.

5 Standard correlations

We now demonstrate that classical semi-empirical Nusselt correlations in the literature map onto the general form (55). Table 3 provides the mapping overview. Three correlations are examined in more detail below: Dittus–Boelter as the uncorrected baseline, Bishop et al. as a representative of formulation using modified Prandtl number, and Swenson et al. correlation as the principal example of wall evaluated corrections. The remaining correlations are summarised afterwards.

5.1 Dittus–Boelter (1930)

The constant-property baseline correlation by [34],

$$\mathrm{Nu} = 0.023\,\mathrm{Re}^{0.8}\,\mathrm{Pr}^{0.4}, \tag{56}$$

evaluates all properties at the bulk temperature T_b and uses no correction factors: $p = q = r = 0$. This is the baseline of (55) with all corrections set to unity. It is valid only when $\mathrm{Pr}_w \approx \mathrm{Pr}_b$ and $\rho_w \approx \rho_b$.

Note that the exponent $n = 0.8$ is not a first-principles result. As shown in [31], the Lyon integral combined with the Prandtl–von Kármán log-law friction factor yields $\mathrm{Nu} \sim \mathrm{Re}/\ln \mathrm{Re}$, whose local power-law exponent $n_{\mathrm{eff}} = 1 - 1/\ln \mathrm{Re}$ lies in the range 0.89–0.93 for $10^4 \leq \mathrm{Re} \leq 10^6$. The lower empirical value $n = 0.8$ absorbs thermal development effects and Re–Pr coupling present in the original calibration datasets into a single power-law fit. The correlation by [32, 51] avoids this compression by retaining the logarithmic friction structure.

Near T_{pc}, the positive Prandtl exponent ($m = 0.4$) is the source of the significant enhancement in predicted Nu whereas in reality the wall heat transfer is unaffected by the bulk property peak. The framework explains this immediately: without the thermal barrier correction ($p = 0$), the correlation has no mechanism to sense the wall-side thermal impedance.

5.2 Bishop et al. (1964)

The correlation by [27],

$$\mathrm{Nu}_b = 0.0069\,\mathrm{Re}_b^{0.9}\,\overline{\mathrm{Pr}}_b^{0.66}\left(\frac{\rho_w}{\rho_b}\right)^{0.43}\left(1 + 2.4\,\frac{d}{x}\right), \tag{57}$$

was developed from experiments in 2.54 and 5.08 mm tubes and the data-based calibration provided: $r = 0.43$, with q and p entangled through $\overline{\mathrm{Pr}}_b$. The higher density-ratio exponent (versus Jackson's 0.3) reflects stronger momentum–energy coupling in small-diameter geometries. The increased exponent $m = 0.66$ on $\overline{\mathrm{Pr}}_b$ compensates for the $\bar{c}_p$ artefact embedded in the modified Prandtl number. The factor $(1 + 2.4\,d/x)$ is an empirical entrance correction, accounting for the thermally developing region near the tube inlet, where the boundary layer has not yet reached the fully developed state.

Correlation	T_{ref}	C	n	m	p	q	r
[34]	T_b	0.023	0.8	0.4	0	0	0
[37]	T_b	0.023	0.8	0.8	†	0	0
[35]	T_f	$0.0277C_l$	0.8	0.36	0.11	0	0
[27]	T_b	0.0069	0.9	$0.66^{\ddagger}$	$0^{\ddagger}$	‡	0.43
[17]	T_w	0.00459	0.923	$0.613^{\ddagger}$	(abs.)	‡	0.231
[38]¶	T_b	(P–K)	∗	∗	$0^{\P}$	$n(T)$	0.3–0.4
[39]	T_b	0.65	0.5	0.34	0.25	0	0
[36]	T_f	(P–K)	∗	∗	0.11	0	0
[24]	T_b	0.0183	0.82	$0.5^{\ddagger}$	$0^{\ddagger}$	$n(T)$	0.3
[40]	T_b	(P–K)	∗	∗	0	0	$0.4^{\S}$

(P–K) = Petukhov–Kirillov base; ∗ = implicit in P–K structure; † = see §5.4;
‡ = entangled with $\bar{c}_p$ through use of $\overline{\mathrm{Pr}}_b = \bar{c}_p\,\mu_b/\lambda_b$; (abs.) = absorbed by wall evaluation; § = in friction law.
¶ = shows $p = 0$ explicitly, but the thermal barrier effect is partially entangled into the regime-dependent exponent $q = n(T)$ with the $\bar{c}_p/c_{p,b}$ factor.

Table 3: Unified mapping of empirical correlations onto the general form (55). Columns p, q, r are the exponents on $(\mathrm{Pr}_b/\mathrm{Pr}_w)$, $(\bar{c}_p/c_{p,b})$, and (ρ_w/ρ_b) respectively.

5.3 Swenson et al. (1965)

The correlation by [17],

$$\mathrm{Nu}_w = 0.00459\,\mathrm{Re}_w^{0.923}\,\overline{\mathrm{Pr}}_w^{0.613}\left(\frac{\rho_w}{\rho_b}\right)^{0.231}, \tag{58}$$

evaluates dimensionless groups at T_w.

The thermal barrier could be better approximated because Pr is evaluated as $\overline{Pr}_w = \frac{\bar{c}_p\,\mu_w}{\lambda_w}$. The price is increased circularity: quantities mainly depend on the unknown T_w, and when $T_w \approx T_{pc}$ all wall-based properties lie in the region of maximum sensitivity. [20] documented the resulting "outbursts" in predicted values, a direct manifestation of the Q-method convergence pathology identified in Section 1. However, when the region of maximum property sensitivity is narrow relative to the axial discretisation, the Swenson-type formulation can yield reasonable predictions provided the mesh spacing allows stable stepping across the pseudocritical zone without resolving its internal structure. The iteration then effectively averages over the sharp property gradients rather than tracking them pointwise, suppressing the Q-method convergence pathology by under-resolution. The trade-off is that any heat transfer deterioration associated with the pseudocritical crossing is necessarily smoothed out: the model cannot predict HTD, but the integrated wall temperature may remain qualitatively acceptable outside the deterioration zone.

It is worth noting that Re_w is commonly obtained from $\mathrm{Re}_b\,(\mu_b/\mu_w)$, so the viscosity ratio $(\mu_w/\mu_b)^n$ is already implicit in any Q-mode calculation. Correlations that carry an explicit viscosity-ratio factor, such as the [52] type, therefore share with the Swenson formulation the same approximation of the momentum-field modification by near-wall property variation; the two approaches differ only in whether this modification is absorbed into the Reynolds-number exponent or retained as a separate multiplicative correction.

5.4 Summary of the remaining correlations

The remaining correlations in Table 3 confirm and extend the classification. [37] ($\mathrm{Nu}_b = 0.023\,\mathrm{Re}_b^{0.8}\,\mathrm{Pr}_{\mathrm{min}}^{0.8}$) selects $\mathrm{Pr}_{\mathrm{min}}$ discretely between wall and bulk with no intermediate values; the elevated exponent $m = 0.8$ absorbs what would otherwise appear as a separate Prandtl-ratio correction, and the resulting kink at $\mathrm{Pr}_w = \mathrm{Pr}_b$ produces discontinuities in Q-method iteration. [35] ($p = 0.11$, $q = 0$,

$r = 0$, $m = 0.36$) and [36], who extended the Petukhov–Kirillov base to lower Reynolds numbers with an identical film-temperature correction structure, independently confirm the same correction architecture under subcritical conditions, the reduced Prandtl exponent being consistent with high-Pr sublayer thinning. The Mikheev–Žukauskas external-flow correlation [39, 53] carries $C = 0.65$, $n = 0.5$, $m = 0.34$ and $p = 0.25$, estimated from crossflow data for air, water, and transformer oil [39, 54, 55]. The [38] and [56] formulation uses $p = 0$, $q = n(T)$, $r = 0.3$–0.4: the $\bar{c}_p/c_{p,b}$ factor does double duty as both the enthalpy–temperature conversion and a partial surrogate for the wall-side property mismatch, forcing the exponent n to vary from 0.4 to 0.7 across five sub-regimes. The Petukhov–Kurganov Reynolds-analogy formulation by [40], expressed directly as an enthalpy Stanton number St_h, avoids the $\bar{c}_p/c_{p,b}$ artefact by construction.

Correlations built on the modified Prandtl number $\overline{\mathrm{Pr}}_b = \bar{c}_p\,\mu_b/\lambda_b$, among them [27] and [24], absorb the $\bar{c}_p/c_{p,b}$ factor into the Prandtl number:

$$\overline{\mathrm{Pr}}_b^{\,m} = \left(\frac{\bar{c}_p}{c_{p,b}}\right)^m \mathrm{Pr}_b^m. \tag{59}$$

The exponent m then simultaneously controls the physical Prandtl dependence from the impedance integral and the bookkeeping conversion $\bar{c}_p/c_{p,b}$, two unrelated effects forced into a single parameter. This is the structural reason why these correlations require regime-dependent exponents near T_{pc}: the bookkeeping factor diverges where c_p peaks, but the integral physics does not.

The impedance integral and the analysis in the previous sections suggest that the impedance should be separated along the pseudocritical isotherm to better account for separate thermodynamic states. This is developed in the next section.

6 The pathway model as two-point quadrature of the impedance integral

When the pseudocritical isotherm lies at radial position r_{pc} within the boundary layer, the impedance integral (23) can be split into wall-side and bulk-side contributions:

$$Z_{\text{total}} = \underbrace{\int_0^{r_{pc}} \frac{R\,\phi(r)/r}{\Gamma_{\text{eff}}(r)\,c_p\big(T(r)\big)}\,\mathrm{d}r}_{Z_{\text{wall-side}}} + \underbrace{\int_{r_{pc}}^{R} \frac{R\,\phi(r)/r}{\Gamma_{\text{eff}}(r)\,c_p\big(T(r)\big)}\,\mathrm{d}r}_{Z_{\text{bulk-side}}}. \tag{60}$$

In each sub-integral, the effective transport coefficient is dominated by one thermodynamic state: Γ_{eff} evaluated near T_w for the wall-side and near T_b for the bulk-side. The thermal barrier zone, centred on r_{pc} where $T(r) = T_{pc}$, straddles the split point; its integrated impedance is distributed across both sub-integrals. The two-point quadrature introduced below replaces the continuous integral by endpoint evaluations and thereby absorbs the barrier's contribution into the pathway conductances.

Applying the thin-sublayer approximations $\phi(r) \approx 1$ and $R/r \approx 1$ within the impedance-controlling region, and evaluating Γ_{eff} at the respective endpoint temperatures, the two sub-integrals yield two pathway impedances Z_w and Z_b.

For the conditions considered here, the total conductance is approximated as a weighted sum of two pathway conductances:

$$G_{\text{total}} = w\,g(\mathrm{Pr}_w) + (1-w)\,g(\mathrm{Pr}_b), \tag{61}$$

where $g(\mathrm{Pr})$ is the conductance function for each pathway and $w \in [0,1]$ is a weight representing the fractional conductance contribution of the wall-side pathway.

In the limit of pure molecular transport (no turbulent bypass), the zones would be strictly in series with $G = 1/(Z_w + Z_b) \leq w\, g_w + (1-w)\, g_b$, the series (harmonic) composition representing the model lower bound. The choice of composition rule matters only beyond first order: the weighted harmonic (series), geometric and arithmetic (parallel) means of the two endpoint conductances coincide to first order in $\xi = \ln(\mathrm{Pr}_b/\mathrm{Pr}_w)$, so the linearised form derived below is composition-independent. The parallel (arithmetic) form (61) is adopted deliberately as the upper envelope of the admissible compositions; the envelope-exceedance diagnostic of the companion paper (Section 2) is therefore a conservative test.

Based on the experimental data, the bounds of (61) are analysed and evaluated against the true conductance in Section 2 of the companion paper [23].

6.1 The Re-dependence and the pathway Nusselt number

In the Dittus–Boelter correlation the exponents n and m emerge together from the coupled $0.023\,\mathrm{Re}^n\mathrm{Pr}^m$ factorisation and are not independently derivable; see [31] for the detailed derivation and discussion. The pathway construction instead separates the two dependences, writing the conductance of each pathway as a product

$$G_i = f(\mathrm{Re})\, g(\mathrm{Pr}_i), \qquad i \in \{w, b\}, \tag{62}$$

in which $f(\mathrm{Re})$ carries the turbulent mixing contribution, common to both pathways, and $g(\mathrm{Pr}_i)$ carries the Prandtl-number dependence of the wall- and bulk-side near-wall resistances separately. The Reynolds dependence thus enters through the single factor $f(\mathrm{Re})$, whose form is set by the flow regime: $f(\mathrm{Re}) \sim \mathrm{Re}/\ln \mathrm{Re}$ in the fully developed regime (Section 6.1.1) and $f(\mathrm{Re}) = C\sqrt{\mathrm{Re}}$ in the barrier-dominated, thermally developing regime (Section 6.1.4).

6.1.1 The fully developed result: $\mathrm{Nu} \sim \mathrm{Re}_\tau$ after pathway absorption

We start from the thin-sublayer impedance integral (30) and convert to wall units. Introduce the friction velocity $u_\tau = \sqrt{\tau_w/\bar{\rho}_w}$ and the wall coordinate $y^+ = y\, u_\tau/\nu_w$, so that $\mathrm{d}y = (\nu_w/u_\tau)\,\mathrm{d}y^+$. The impedance becomes

$$Z_{\mathrm{total}} = \frac{\nu_w}{u_\tau\, \lambda_w} \int_0^{\delta^+} \frac{\lambda_w/\lambda\big(T(y^+)\big)}{1 + \eta(y^+, T)}\, \mathrm{d}y^+. \tag{63}$$

The dimensionless impedance integral is $\mathcal{I} = \int_0^{\delta^+} [\lambda_w/\lambda(T(y^+))]\,[1 + \eta(y^+, T)]^{-1}\ \mathrm{d}y^+$, and the Nusselt number based on bulk conductivity is

$$\mathrm{Nu}_b = \mathrm{Re}_{\tau,w}\, \frac{\lambda_w}{\lambda_b}\, \frac{1}{\mathcal{I}}, \tag{64}$$

where $\mathrm{Re}_{\tau,w} = u_\tau\, d/\nu_w$. No friction-factor model has been assumed; the result is exact within the thin-sublayer approximation.

The pathway model replaces $1/\mathcal{I}$ by the parallel conductance (61):

$$\mathrm{Nu}_b = \mathrm{Re}_{\tau,w}\, \frac{\lambda_w}{\lambda_b}\, \left[\, w\, \mathrm{Pr}_w^{-\beta} + (1-w)\, \mathrm{Pr}_b^{-\beta}\, \right]. \tag{65}$$

All Pr-dependent physics is now in the bracket.

6.1.2 The friction Reynolds number without empirical friction laws

From the momentum balance,

$$\mathrm{Re}_{\tau,w} = \mathrm{Re}_b \, \frac{\mu_b}{\mu_w} \sqrt{\frac{f}{8}} \sqrt{\frac{\rho_w}{\rho_b}}, \tag{66}$$

and the Prandtl–von Kármán relation for fully developed turbulent pipe flow,

$$\frac{1}{\sqrt{f}} = \frac{1}{2\kappa} \ln\!\left(\mathrm{Re}_b \sqrt{f}\,\right) + B, \tag{67}$$

where $\kappa \approx 0.41$ and B is a constant, it follows that in the limit of large Re, where $\sqrt{f/8} \sim 1/\ln \mathrm{Re}_b$,

$$\mathrm{Nu}_{\mathrm{f.d.}} \;\sim\; \frac{\mathrm{Re}}{\ln \mathrm{Re}} \left[\, w\, g(\mathrm{Pr}_w) + (1-w)\, g(\mathrm{Pr}_b) \,\right]. \tag{68}$$

This scaling is nearly linear in Re, with an effective exponent $n_{\mathrm{eff}} = 1 - 1/\ln \mathrm{Re}$ that increases from the Dittus–Boelter value $n \approx 0.8$ toward $n \to 1$ as $\mathrm{Re} \to \infty$, consistent with the higher exponents used by [27] ($n = 0.9$) and [17] ($n = 0.923$); see Table 3; the detailed derivation and discussion are given in [31].

6.1.3 Breakdown of the fully developed assumption at the pseudocritical barrier

The capacitive, history-dependent, and lagging features of the impedance integral anticipated in Section 3 are made quantitative here and in Section 6.1.4.

A remark on the domain of validity is in order, since the impedance integral (21) is derived under the fully developed assumption whose breakdown this subsection establishes. The resolution is as follows: the radial structure of the integrand is retained quasi-locally – frozen at each axial position – and this fixes the Prandtl-number structure of Sections 3.2 and 6, which depends only on the instantaneous property distribution across the boundary layer. The Reynolds-number scaling, by contrast, encodes the axial equilibrium of the thermal profile and cannot be taken from the integral once that equilibrium is lost; it is re-derived independently from the penetration argument of Section 6.1.4.

The fully developed scaling (68) rests on the assumption that the axial enthalpy gradient is uniform across the pipe radius. When the pseudocritical isotherm lies within the boundary layer ($0 < \theta_{pc} < 1$), where

$$\theta_{pc} = (T_{pc} - T_b)/(T_w - T_b) \tag{69}$$

is the barrier position which locates the pseudocritical isotherm within the wall-to-bulk interval, the fully developed assumption is violated locally.

The barrier creates a zone of sharply elevated thermal impedance. As the bulk temperature rises along the pipe, θ_{pc} moves continuously and the barrier sweeps radially through the boundary layer. At each axial position where θ_{pc} transitions through the interval [0, 1], the temperature profile must re-develop from the barrier position outward. This re-development is an internal thermal effect induced by the moving pseudocritical barrier. Unlike the classical entrance region, which occurs once at the pipe inlet, the barrier-induced re-development is renewed at every axial position where the barrier position shifts. The thermal profile never reaches the fully developed equilibrium that underlies (68).

Two features of the experimental data used in Section 2 of the companion paper Otić and Ertunç [23] show this directly: (1) the bulk Reynolds number changes by up to a factor of three between pipe inlet and outlet; (2) the wall-temperature peaks associated with HTD occur precisely in the axial zone where θ_{pc} passes through the interval [0, 1].

Since the fully developed assumption is violated in the barrier-dominated regime, the Re-scaling in this regime cannot be derived from the integral. We therefore derive an independent scaling estimate based on the penetration depth of the thermal disturbance. The impedance integral remains the origin of the Pr-dependence, only the Re-scaling requires a different physical argument.

6.1.4 The penetration scaling in the barrier-dominated regime

In the barrier-dominated regime the equilibrium logarithmic layer that underlies the fully developed relation $\mathrm{Re}_{\tau,w} \sim \mathrm{Re}/\ln \mathrm{Re}$ is absent, and the common factor $f(\mathrm{Re})$ of (62) is governed by the factored impedance integral (31). In the following we show that the penetration of the thermal front across the barrier sets the Reynolds exponent, while the Nusselt number and its Prandtl dependence follow, as throughout this work, from the impedance integral (64).

When the thermal profile is locally developing, the appropriate scaling is the penetration-depth estimate for the thermal boundary layer growing from the barrier into the turbulent core. Consider an advected fluid element past an axial location at which the pseudocritical barrier, at the radial position r_{pc} of (69), lies within the boundary layer. The fluid element resides at a position for a convective time $t_{\mathrm{res}} \sim d/\tilde{u}_b$ and the disturbance diffuses the barrier penetration depth over the convective time as $\delta_{\mathrm{pen}} \sim (\varepsilon_{h,\mathrm{barrier}}\, t_{\mathrm{res}})^{1/2}$,

$$\delta_{\mathrm{pen}} \sim \sqrt{\varepsilon_{h,\mathrm{barrier}}\, \frac{d}{\tilde{u}_b}}. \tag{70}$$

The ratio of advective to diffusive transport across the barrier defines the barrier Péclet number

$$\mathrm{Pe}_t \equiv \frac{\tilde{u}_b\, d}{\varepsilon_{h,\mathrm{barrier}}}. \tag{71}$$

A single-scale penetration estimate of this kind cannot be read directly as a Nusselt number, since every dimensionally consistent version of it retains a Prandtl number. The conductance density of the factored integrand (31) is $\lambda(1+\eta)$, with $\eta = \varepsilon_h\,\mathrm{Pr}/\nu$ from (32), and the admissible pairings of diffusivity scale and conductance establish the point. At the barrier the sharp property peak damps the turbulent transport, but it does not extinguish it: the turbulent momentum diffusivity is reduced toward its kinematic floor, $\varepsilon_{m,\mathrm{barrier}} \sim \nu$, and with $\mathrm{Pr}_t = O(1)$ the same holds for the turbulent thermal diffusivity, consistent with the DNS evidence of strong turbulent heat-flux damping across the pseudocritical layer [45, 46]. Were the barrier transport genuinely molecular ($\eta \ll 1$), the front would diffuse with the thermal diffusivity, $\delta_{\mathrm{pen}} \sim (\alpha\, d/\tilde{u}_b)^{1/2}$, and the molecular conductance would yield $\mathrm{Nu} \sim (\mathrm{Re}\,\mathrm{Pr})^{1/2}$, the constant-property plug-flow result of Appendix B. Were it instead governed by the kinematic scale, $\varepsilon_{h,\mathrm{barrier}} \sim \nu$ and $\delta_{\mathrm{pen}} \sim (\nu\, d/\tilde{u}_b)^{1/2}$, the accompanying enhancement $(1+\eta) \sim (1+\mathrm{Pr})$ would reappear in the conductance and return $\mathrm{Nu} \sim \mathrm{Pr}\,\mathrm{Re}^{1/2}$, see Appendix B.

The Reynolds scaling of the penetration width is most transparent in outer variables. A front carried across the barrier by transport of kinematic scale $\varepsilon_{h,\mathrm{barrier}} \sim \nu$ over the residence time $t_{\mathrm{res}} \sim d/\tilde{u}_b$ reaches

$$\frac{\delta_{\mathrm{pen}}}{d} \sim \left(\frac{\nu}{\tilde{u}_b\, d}\right)^{1/2} = \mathrm{Re}^{-1/2}, \tag{72}$$

the growth law of a thermal layer developing under uniform advection over a streamwise length of order the pipe diameter. The exponent is that of the uniform-advection branch of Appendix B and is insensitive to the precise development length: replacing d by an axial scale L rescales δ_{pen}/d by

$(L/d)^{1/2}$, which is absorbed into the constant C and leaves the exponent unchanged. In wall units the same statement reads $\delta^+_{\mathrm{pen}} \sim (f/8)^{1/2}\,\mathrm{Re}^{1/2}$, in which the friction factor enters only through the viscous length ν/u_τ that non-dimensionalises the wall-normal coordinate. It cancels identically against the friction factor in $\mathrm{Re}_{\tau,w} = (f/8)^{1/2}\mathrm{Re}$ when the Reynolds factor of the impedance integral (64) is formed,

$$f(\mathrm{Re}) = \frac{\mathrm{Re}_{\tau,w}}{\delta^+_{\mathrm{pen}}} = \frac{d}{\delta_{\mathrm{pen}}} \sim \mathrm{Re}^{1/2}. \tag{73}$$

Unlike the fully developed branch, which requires the Prandtl–von Kármán relation (67) to convert $\mathrm{Re}_{\tau,w}$ into $\mathrm{Re}/\ln\mathrm{Re}$, the barrier branch invokes no friction correlation. The friction factor is a bookkeeping quantity that enters and leaves with the choice of variables, and the penetration form $f(\mathrm{Re}) = C\sqrt{\mathrm{Re}}$ therefore carries no Prandtl number by construction. The Prandtl dependence of the pathway Nusselt number originates instead in the molecular sublayer, whose wall-referenced thickness $y_c^+ \sim (\mathrm{Pr}_t/\mathrm{Pr}_w)^{1/3}$ of (34) sets the near-wall conductance $g(\mathrm{Pr}_i)$ recombined in Section 6.1.5. It is distinct in both origin and sign from the $(\mathrm{Re}\,\mathrm{Pr})^{1/2}$ of the plug-flow limit.

The physical picture is transparent. In the fully developed regime the entire wall-to-centre turbulent diffusivity participates, $\varepsilon_h \sim \nu\,\mathrm{Re}_\tau$, the impedance accumulates over the full logarithmic layer, and $f(\mathrm{Re})$ takes the equilibrium form $\mathrm{Re}/\ln\mathrm{Re}$ of (68). When the pseudocritical barrier damps turbulent transport and continuously resets the thermal profile, the logarithmic contribution is truncated, the effective penetration diffusivity collapses from $\varepsilon_h \sim \nu\,\mathrm{Re}_\tau$ toward its kinematic floor ν, and $f(\mathrm{Re})$ reverts to the developing-flow $\sqrt{\mathrm{Re}}$. This is the uniform-advection (plug-flow) counterpart of the Lévêque–Graetz mechanism [48, 49], which yields the penetration exponent $1/2$ rather than the shear-driven $1/3$, driven here by internal thermal re-development rather than by the classical pipe inlet. The solvable constant-property limit is given in Appendix B.

That a $1/2$ exponent should arise when the thermal boundary layer does not reach its fully developed equilibrium is not peculiar to the present problem. Kraichnan [41] predicted an asymptotic $\mathrm{Nu} \sim \mathrm{Ra}^{1/2}(\ln\mathrm{Ra})^{-3/2}$ for turbulent free convection, the ultimate regime in which the boundary layers themselves become turbulent; more recently, Zhu et al. [42] showed by direct numerical simulation that multiscale wall roughness holds the thermal boundary layer in a transitional state, successively smaller roughness scales protruding through it as the Rayleigh number rises, and sustains an effective $\mathrm{Nu} \sim \mathrm{Ra}^{1/2}$ over three decades of Ra, a state distinguished from the asymptotic ultimate regime. The forcing, the perturbing structure and the resulting boundary-layer state all differ from the Rayleigh–Bénard case. The operative principle is nonetheless shared: once the molecular-diffusive boundary resistance is bypassed, whether by turbulent boundary layers, by roughness protrusion or by continual axial re-development, transport follows a square-root law, with exponent $1/2$ in place of the fully developed $\mathrm{Re}/\ln\mathrm{Re}$.

Closer to the present forced-convection setting, the dependence of the heat-transfer exponent on the state of the boundary layer recurs in wall-bounded flow: for rough-wall turbulent channel flow with a logarithmic boundary layer, MacDonald et al. [57] report an effective exponent $\beta \approx 0.42$, well away from the smooth-wall value. The control parameter and the mechanism differ from the present penetration regime, but the theory holds across the free and forced branches alike: the leading-order exponent is set by the state of the thermal boundary layer, not fixed at its fully developed value.

What the quadrature captures and what it neglects. The two-point approximation (61) captures the variation of Γ_{mol} between wall and bulk. It does not separately resolve the property-fluctuation correlations or the turbulent Prandtl number variation absorbed by Γ_{eff}.

The two scalings are limiting regimes of the same physics:

Regime	Effective n	Condition
Fully developed (no barrier)	$n \to 1 - O(1/\ln \mathrm{Re})$	$\theta_{pc} \notin [0,\, 1]$
Barrier-dominated (developing)	$n \to 1/2$	$\theta_{pc} \in [0,\, 1]$, strong barrier

This regime dependence is confirmed by the extended validation database (Section 3.4 (companion paper)) to show that the effective exponent $n_{\mathrm{eff}} = \partial \ln \mathrm{Nu}/\partial \ln \mathrm{Re}$ decreases systematically from the no-crossing cases to the strong-barrier cases (where Re_b varies by up to a factor of three along the pipe and $n = 0.5$ is clearly preferred).

The Prandtl–von Kármán relation (67) rather than a Blasius-type power-law friction factor is used throughout: a fixed-exponent friction law cannot distinguish the fully developed regime ($n_{\mathrm{eff}} \approx 0.9$) from the barrier-dominated regime ($n = 0.5$) identified above, and the conditions considered here lie beyond the Blasius validity range; the argument is given in [31]. A full parametric analysis of $n_{\mathrm{eff}}(\theta_{pc})$ is deferred to a separate study.

The present results establish that $\sqrt{\mathrm{Re}}$ is the appropriate leading-order description in the barrier-dominated regime.

6.1.5 The pathway Nusselt number

In the barrier-dominated, thermally developing regime the factor $f(\mathrm{Re})$ of (62) takes the penetration form $C\sqrt{\mathrm{Re}}$ derived in Section 6.1.4. The conductivity ratio λ_w/λ_b carried by (64) is of order unity across the conditions considered here and is absorbed into the pathway conductances $g(\mathrm{Pr}_i)$; it is not retained as a separate factor. The pathway conductance retains the power-law form

$$g(\mathrm{Pr}) = \mathrm{Pr}^{-\beta}, \qquad \beta > 0, \tag{74}$$

already introduced in (65), in which the resistance exponent β measures the sensitivity of the near-wall conductance to the Prandtl number. Substituting into the parallel-conductance approximation (61) gives the parallel pathway Nusselt number,

$$\mathrm{Nu} = C\sqrt{\mathrm{Re}}\,\left[\, w\,\mathrm{Pr}_w^{-\beta} + (1-w)\,\mathrm{Pr}_b^{-\beta}\,\right], \tag{75}$$

which uses only the standard Prandtl numbers Pr_b and Pr_w and avoids the $\bar{c}_p/c_{p,b}$ artefact. The expression contains two parameters, the pathway weight w and the resistance exponent β, which are the subject of the next two paragraphs. The exponent $n = 1/2$ on Re, by contrast, is not a parameter to be determined: it is the limiting value in the barrier-dominated regime, derived in Section 6.1.4. In the absence of a pseudocritical crossing the fully developed scaling (68) applies and the correlation literature recovers $n \approx 0.8$–0.9.

Pathway weight. The two-point quadrature evaluates the conductance at the wall and bulk endpoints, Pr_w and Pr_b, which locate the two thermodynamic states bounding the boundary layer. Alongside the bulk-referenced barrier position (69) one can introduce its wall-referenced counterpart,

$$\theta_{pc}^{w} = \frac{T_{pc} - T_w}{T_w - T_b} = \theta_{pc} - 1, \tag{76}$$

so that $\theta_{pc} = 0$ marks the bulk crossing ($T_b = T_{pc}$) and $\theta_{pc}^{w} = 0$ marks the wall crossing ($T_w = T_{pc}$). These are the two zero crossings between which the pseudocritical barrier sweeps through the boundary layer.

Within the two-point quadrature the wall and bulk endpoints enter through the same conductance function $g(\mathrm{Pr})$, and the barrier resistance spanning the pseudocritical region is, to leading

order, Pr-independent (Eq. (43)). Once the barrier is Pr-independent, the quadrature contains no internal information that distinguishes the two endpoints, and the weight assignment must not favour either of them. To make this indifference requirement explicit it is convenient to write the conductance bracket in terms of the logarithmic Prandtl ratio $\xi = \ln(\mathrm{Pr}_b/\mathrm{Pr}_w)$. Factoring $\mathrm{Pr}_b^{-\beta}$ out of (75) and using the identity $\mathrm{Pr}_w^{-\beta} = \mathrm{Pr}_b^{-\beta}\, e^{\beta\xi}$ yields

$$\mathrm{Nu}_b = C\sqrt{\mathrm{Re}_b}\,\mathrm{Pr}_b^{-\beta}\,\underbrace{\left[\, w\, e^{\beta\xi} + (1-w)\,\right]}_{\mathcal{F}(\xi;\, w)}, \tag{77}$$

where, with $\xi = \ln(\mathrm{Pr}_b/\mathrm{Pr}_w)$, the identity $\mathrm{Pr}_w^{-\beta} = \mathrm{Pr}_b^{-\beta}\, e^{\beta\xi}$ is immediate. The endpoint interchange reverses the sign of ξ and simultaneously exchanges the weights of the two pathways, inducing the mapping

$$\mathcal{F}(\xi;\, w) \;\longmapsto\; e^{-\beta\xi}\,\mathcal{F}(\xi;\, 1-w). \tag{78}$$

A weight assignment indifferent to the endpoint labelling requires the bracket to be form-invariant under this mapping, which demands $w = 1 - w$, that is,

$$w = \tfrac{1}{2}. \tag{79}$$

The equal-weight choice is the unique unbiased assignment available to the quadrature once the barrier has been shown to contribute a Pr-independent resistance. It is an indifference argument, not a symmetry of the physical configuration: the squared mass-flux weighting in the generalised Lyon integral (21) and the molecular sublayer at the wall are not wall/bulk-symmetric, and any systematic departure from (79) must originate there. The assignment is therefore confirmed empirically: the data-based evaluation in Section 2 of the companion paper recovers (79) at the bulk crossing $\theta_{pc} = 0$ across all fluids and Reynolds numbers and characterises the controlled departure from $w = 1/2$ as the barrier sweeps through the boundary layer.

Resistance exponent. The two asymptotic regimes derived in Section 3.2.3 bound β:

Regime	**Conductance**	**Effective** β
Classical sublayer (no barrier)	$g \propto \mathrm{Pr}^{-2/3}$	$\beta = 2/3$
Barrier-dominated ($Z_{\mathrm{barrier}} \gg Z_{\mathrm{sublayer}}$)	$g \propto \mathrm{Pr}^{0}$	$\beta \to 0$

These bounds are derived under the fully developed assumption of the generalised Lyon integral; they constrain β to the open interval $(0,\, 2/3)$ but do not select a specific value. The selection is taken from the empirical correlation tradition that shares the linearised structure $\mathrm{Pr}_b^{-\beta}(\mathrm{Pr}_b/\mathrm{Pr}_w)^p$ and whose exponents were calibrated under conditions of moderate, approximately symmetric property variation, for which the unbiased weight $w = 1/2$ holds independently of the conductance function: the Mikheev correlation and its external-flow refinement by Žukauskas [39, 53] adopt $p = 0.25$. Inverting $p = w\beta$ at $w = 1/2$ gives

$$\beta = \frac{p}{w} = \frac{0.25}{0.50} = 0.50. \tag{80}$$

This value lies within the theoretical interval $(0,\, 2/3)$ derived in §3.2.3, closer to the barrier-dominated end than to the sublayer end, consistent with the regime in which the linearised form is intended to apply. It is fixed a priori from this external-empirical prior and is not adjusted anywhere

in the present work; the impedance-ratio test of Section 2 in the companion paper provides the primary, database-wide support for the choice. The Prandtl-ratio exponent in the general form (55) is therefore

$$p = w\beta = \tfrac{1}{4}. \tag{81}$$

The retention of $\beta = 1/2$ in the strongly variable-property, barrier-dominated regime is a non-trivial prediction of the framework rather than a fit, and is tested as such in §2 of the companion paper through the impedance-ratio comparison.

The linearised pathway form. With $w = 1/2$ derived and $\beta = 1/2$ fixed, the parallel pathway Nusselt number (75) reduces to the linearised pathway form. To exhibit this reduction, we expand the bracket function $\mathcal{F}(\xi;\, 1/2)$ for property variation ξ:

$$\mathcal{F}(\xi;\, \tfrac{1}{2}) = \tfrac{1}{2}e^{\beta\xi} + \tfrac{1}{2} = 1 + \tfrac{1}{2}\beta\,\xi + \tfrac{1}{4}\beta^2\,\xi^2 + O(\xi^3). \tag{82}$$

The first-order term is precisely the linear part of $e^{w\beta\xi}$ at $w = 1/2$. Replacing the bracket function by its first-order exponential approximation,

$$\mathcal{F}(\xi;\, \tfrac{1}{2}) \;\approx\; e^{w\beta\xi} = \left(\frac{\mathrm{Pr}_b}{\mathrm{Pr}_w}\right)^{w\beta} = \left(\frac{\mathrm{Pr}_b}{\mathrm{Pr}_w}\right)^{1/4}, \tag{83}$$

substituting back into (77), and writing the result with the bulk-referenced Reynolds and Prandtl numbers, yields the linearised pathway form

$$\mathrm{Nu}_b = C\sqrt{\mathrm{Re}_b}\;\mathrm{Pr}_b^{-1/2}\left(\frac{\mathrm{Pr}_b}{\mathrm{Pr}_w}\right)^{1/4} \tag{84}$$

with C of order unity by construction; $C = 1$ is adopted and tested uncalibrated in the companion paper. We refer to this expression as LinP throughout. It carries no modified Prandtl number, no $\bar{c}_p/c_{p,b}$ factor, no fitted coefficient, and no density-ratio correction.

The linearisation (83) is the source of the LinP designation: it replaces the parallel-conductance bracket (77) by its first-order exponential approximation and is exact in the limit $\xi \to 0$. The quality of this approximation across the full range of property variation encountered in supercritical conditions is quantified in Section 2 of the companion paper through the bracket function $\mathcal{F}_{\mathrm{exp}}$ extracted from the experimental database. The departure of $\mathcal{F}_{\mathrm{exp}}$ from $\mathcal{F}_{\mathrm{LinP}}$ in the strongly contrasted regime, identified there, motivates the extension of the linearised form by a pathway-resolved density correction, which is left to a separate work.

7 Summary and open problems

7.1 Summary

When the pseudocritical barrier lies within the boundary layer, its radial sweep transforms the constant-property Lyon integral from a thermal resistance into a thermal impedance. This structural change, derived from the Favre-averaged energy equation, accounts for the property-ratio correction factors that six decades of correlation development have introduced empirically: the Prandtl, density, and integrated specific-heat ratios arise from distinct terms of one impedance integrand. Three principal results were established.

First, the generalised Lyon integral (21) and the decomposition of the effective transport coefficient $\Gamma_{\mathrm{eff}} = \Gamma_{\mathrm{mol}} + \Gamma_{\mathrm{turb}}$ provide a classification of the correction factors by their physical origin

(Table 2). The constant-property Lyon integral is a thermal *resistance* – a real-valued, history-independent quantity evaluated once for a given (Re, Pr) pair; the variable-property generalisation is a thermal *impedance*, distinguished by capacitive thermal storage at the c_p peak, history dependence through the axially sweeping pseudocritical barrier, and response lag in the perpetually developing thermal profile.

(i) The integrated specific heat ratio $(\bar{c}_p/c_{p,b})^q$ is an artefact of converting enthalpy differences to temperature differences in the global energy balance; it is external to Γ_{eff} and eliminable by working in an enthalpy-based formulation.

(ii) The Prandtl ratio $(\mathrm{Pr}_b/\mathrm{Pr}_w)^p$ arises from the balance between two components of the impedance integral: the molecular sublayer resistance, which scales as $\mathrm{Pr}_w^{2/3}$, and the thermal barrier resistance at the pseudocritical isotherm, which was shown to be independent of Pr to leading order (Eq. (43)). The barrier zone is memoryless in isolation; the impedance character of the total wall-to-bulk transport arises from the barrier's radial sweep. The power-law parameterisation $(\mathrm{Pr}_b/\mathrm{Pr}_w)^p$ approximates the transition from sublayer-dominated ($p \to 2/3$) to barrier-dominated ($p \to 0$) regimes.

(iii) The density ratio $(\rho_w/\rho_b)^r$ arises from the modification of Γ_{turb} through density-driven velocity redistribution, which alters the turbulent bypass factor $1/(1+\eta)$ in the integrand without directly affecting the molecular impedance.

Ten classical correlations [17, 24, 27, 34–40] were shown to map onto a single general structure (55) differing only in the choice of reference temperature, exponent values, and degree of entanglement between the factors (Table 3). The entanglement of the $\bar{c}_p/c_{p,b}$ artefact with the Prandtl correction through the modified Prandtl number $\overline{\mathrm{Pr}}_b = \bar{c}_p\,\mu_b/\lambda_b$ was identified as a mechanism responsible for spurious behaviour near the pseudocritical temperature: the artefact factor diverges at T_{pc} because $\bar{c}_p$ inherits the c_p peak, whereas the physical sublayer–barrier correction is bounded because the barrier resistance is Pr-independent to leading order. A single exponent on $\overline{\mathrm{Pr}}_b$ cannot simultaneously represent a bounded physical effect and an unbounded artefact, which is the structural reason why entangled correlations require regime-dependent exponent switching adopted in many correlations.

Second, the pseudocritical barrier was identified as the source of the impedance character of the generalised Lyon integral. When the pseudocritical isotherm lies within the boundary layer, the zone of sharply elevated thermal impedance sweeps radially as the bulk temperature rises, continuously resetting the thermal profile so that it never attains the fully developed state: the thermal field is perpetually developing, and the equilibrium underlying the classical $\mathrm{Re}/\ln\mathrm{Re}$ scaling is never established. The resulting penetration-depth scaling replaces that dependence with $\mathrm{Nu} \sim \sqrt{\mathrm{Re}}$ in the barrier-dominated regime – a square-root law with precedent in turbulent thermal convection wherever the molecular-diffusive sublayer ceases to control the wall-to-bulk flux [41, 42, 58], reached here by continual axial re-development. The fully developed limit itself, and the structural rigidity of the calibrated constant-property correlations – the locking of the prefactor 0.023 to the exponent $\mathrm{Re}^{0.8}$, which property-ratio factors on Pr and ρ leave untouched – are established separately [31]; the companion paper confirms the rigidity directly through the collapse of the uncalibrated $\mathrm{Re}^{0.8}\mathrm{Pr}^{0.4}$ baseline onto the bulk temperature (Section 3.3, Part II).

Third, a linearised pathway form was obtained by splitting the impedance integral at the pseudocritical isotherm and applying a two-point quadrature. The resulting expression (84),

$$\mathrm{Nu}_b \approx C\sqrt{\mathrm{Re}_b}\,\mathrm{Pr}_b^{-\beta}\left(\frac{\mathrm{Pr}_b}{\mathrm{Pr}_w}\right)^{w\beta},$$

resolves the Prandtl correction through the ratio $\mathrm{Pr}_b/\mathrm{Pr}_w$ with the symmetric pathway weight $w = 1/2$, the unique unbiased assignment of the two-point quadrature, and the resistance exponent $\beta = 1/2$ fixed a priori from the Mikheev–Žukauskas correlation family [39, 53], consistent with the theoretical bounds $\beta \in (0,\, 2/3)$ derived in Section 3.2.3 and confirmed by the impedance diagnostics of the companion paper. No modified Prandtl number, no $\bar{c}_p/c_{p,b}$ factor, and no regime-dependent switching rules are required. The expression is smooth across the pseudocritical transition by construction and well-conditioned under Q-mode iteration.

The linearised pathway form is the simplest testable consequence of the framework: the Prandtl-ratio exponent, the pathway weight, and the Re-scaling prefactor are predicted rather than fitted, and the functional form is fixed by the derivation. Evaluated uncalibrated against 2201 measurement stations spanning water and CO_2, it carries the lowest case root-mean-square wall-temperature error of the models tested, despite using no fitted parameters and no density correction (Section 3.3 of the companion paper, Part II). The experimental validation, the scope of quantitative validity, and the diagnostic tests of the pathway decomposition are developed in the companion paper ([23], see §1).

7.2 Open problems

Two open problems arise within the framework itself, independent of whatever empirical scope limits the validation will identify.

(i) Turbulent Prandtl number and property-fluctuation correlations. The property-fluctuation correlations and the variation of the turbulent Prandtl number $\mathrm{Pr}_t(r, T)$ under strong property gradients are absorbed into Γ_{eff} but do not map onto any of the three classical correction factors. In Petukhov's limit these effects vanish; near T_{pc} they represent an additional source of uncertainty that is partially absorbed into the empirical exponents of classical correlations but not independently resolved. DNS-based parameterisations of $\mathrm{Pr}_t(r, T)$, along the lines of Günseren et al. [59], would allow this contribution to be isolated and, if significant, incorporated as a fourth correction factor or absorbed into a refined conductance function $g(\mathrm{Pr},\, \mathrm{Pr}_t)$. The pointwise reference-temperature architecture common to all correlations considered here cannot resolve axial turbulence structure that arises on scales beyond the local thermal equilibrium, as exemplified by the axial wall-temperature modulation documented in the companion paper ([23], see §1) for a long heated pipe at $L/d = 400$.

(ii) The circularity problem as a structural limitation. The circularity inherent in predicting T_w from a correlation that depends on T_w through wall-evaluated properties is not a deficiency of any particular correlation but a structural property of the Nusselt-number framework. The linearised pathway form reduces the severity of this problem: the additive conductance structure is better conditioned than multiplicative property-ratio chains, and the elimination of the $\bar{c}_p/c_{p,b}$ divergence removes one feedback mechanism. But the circularity cannot be eliminated as long as the prediction target is $\mathrm{Nu}(T_w)$. Near T_{pc}, where properties are maximally sensitive to temperature, this feedback loop defines an inherent ceiling on the accuracy of any Nusselt-number-based prediction, regardless of how the correction factors are structured. The path beyond this ceiling leads either to enthalpy-based formulations (as the Kurganov–Petukhov St_h approach suggests) or to methods that avoid the T_w-dependent iteration entirely.

A Thermal resistance derivation

The squared-integral form (19) is obtained from (18) by substituting the enthalpy profile (17) and exchanging the order of integration. The derivation is as follows. Substituting (17) into (18):

$$\tilde{h}_w - \tilde{h}_b = \frac{2}{R^2}\int_0^R \underbrace{\left[q_w R \int_r^R \frac{\phi(r')/r'}{\Gamma_{\text{eff}}(r')}\,\mathrm{d}r'\right]}_{\tilde{h}_w - \tilde{h}(r)} \frac{\bar{\rho}(r)\,\tilde{u}(r)}{\bar{\rho}_b\,\tilde{u}_b}\, r\,\mathrm{d}r. \tag{85}$$

This is a double integral over the domain

$$\mathcal{D} = \big\{(r,\, r') : 0 \le r \le R,\;\; r \le r' \le R\big\}. \tag{86}$$

Writing (85) as an iterated integral over $\mathcal{D}$ and interchanging the two integrations (justified by the absolute integrability of the integrand, which is bounded and continuous for $r > 0$):

$$\mathcal{D} = \big\{(r,\, r') : 0 \le r' \le R,\;\; 0 \le r \le r'\big\}, \tag{87}$$

the expression becomes

$$\tilde{h}_w - \tilde{h}_b = \frac{2\,q_w\,R}{R^2}\int_0^R \frac{\phi(r')/r'}{\Gamma_{\text{eff}}(r')} \underbrace{\left[\int_0^{r'} \frac{\bar{\rho}(r)\,\tilde{u}(r)}{\bar{\rho}_b\,\tilde{u}_b}\, r\,\mathrm{d}r\right]}_{(\star)} \mathrm{d}r'. \tag{88}$$

Note that the inner integral $(\star)$ is directly related to the cumulative mass-flux function ϕ. From the definition (11) and the bulk mass-flux identity (8):

$$\int_0^R \bar{\rho}(r)\,\tilde{u}(r)\,r\,\mathrm{d}r = \tfrac{R^2}{2}\,\bar{\rho}_b\,\tilde{u}_b, \tag{89}$$

so that, with $J(r) \equiv \int_0^r \bar{\rho}\,\tilde{u}\,r'\,\mathrm{d}r'$ and $\phi(r') = J(r')/J(R)$ from (11), the inner integral in (88) evaluates to

$$(\star) = \frac{1}{\bar{\rho}_b\,\tilde{u}_b}\int_0^{r'} \bar{\rho}\,\tilde{u}\,r\,\mathrm{d}r = \frac{J(r')}{\bar{\rho}_b\,\tilde{u}_b} = \frac{R^2}{2}\,\phi(r'). \tag{90}$$

Substituting (90) into (88):

$$\begin{aligned}\tilde{h}_w - \tilde{h}_b &= \frac{2\,q_w\,R}{R^2}\int_0^R \frac{\phi(r')/r'}{\Gamma_{\text{eff}}(r')} \cdot \frac{R^2}{2}\,\phi(r')\,\mathrm{d}r' \\ &= q_w\,R\int_0^R \frac{[\phi(r')]^2}{\Gamma_{\text{eff}}(r')\;r'}\,\mathrm{d}r',\end{aligned} \tag{91}$$

which, with the identity $\phi(r) = (2/R^2)\int_0^r (\bar{\rho}\,\tilde{u}/\bar{\rho}_b\,\tilde{u}_b)\,r'\,\mathrm{d}r'$ implied by (89), is the form stated in (19).

The result may be verified against two exact constant-property limits. For constant properties, $\Gamma_{\text{eff}} = (\lambda/c_p)\,(1+\eta)$ with the transport ratio η of (32), $\tilde{h}_w - \tilde{h}_b = c_p\,(T_w - T_b)$, and, in the dimensionless radius $\hat{r} = r/R$ with $\phi(\hat{r}) = 2\int_0^{\hat{r}} (\bar{u}/\bar{u}_b)\,\hat{r}'\,\mathrm{d}\hat{r}'$, equation (91) combined with $\mathrm{Nu} = 2\,R\,q_w/[\lambda\,(T_w - T_b)]$ gives the classical Lyon integral

$$\frac{1}{\mathrm{Nu}} = 2\int_0^1 \frac{1}{\hat{r}\,\big(1+\eta(\hat{r})\big)}\left(\int_0^{\hat{r}} \frac{\bar{u}}{\bar{u}_b}\,\hat{r}'\,\mathrm{d}\hat{r}'\right)^2 \mathrm{d}\hat{r}. \tag{92}$$

With $\eta = 0$ (molecular conduction only) and constant wall heat flux, (92) yields $\mathrm{Nu} = 8$ for slug flow ($\bar{u} = \bar{u}_b$) and $\mathrm{Nu} = 48/11$ for laminar Poiseuille flow ($\bar{u}/\bar{u}_b = 2(1-\hat{r}^2)$), the exact constant-flux results.

B The penetration scaling in a constant-property limit

The penetration estimate of Section 6.1.4 is a scaling argument. A constant-property limit renders it exact, identifies which laminar branch the residence-time construction selects, and shows how the diffusivity scale entering the penetration depth fixes the Prandtl exponent.

The exponent of a developing-layer Nusselt number is set by the velocity profile that the advancing thermal front samples as it grows, with x the distance from the developing position, a the thermal diffusivity, and δ_T the layer thickness. When the front sits in the near-wall shear, $u \approx \dot{\gamma}_w\, y$, the balance $\dot{\gamma}_w\, y\, \partial_x T \sim a\, \partial_{yy} T$ gives the Lévêque–Graetz result [48, 49],

$$\delta_T \sim \left(\frac{a\,x}{\dot{\gamma}_w}\right)^{1/3}, \qquad \mathrm{Nu} \sim \mathrm{Gz}^{1/3} = \left(\mathrm{Re}\,\mathrm{Pr}\,\frac{d}{x}\right)^{1/3}, \tag{93}$$

with $\mathrm{Gz} = \mathrm{Re}\,\mathrm{Pr}\,d/x$, where $\dot{\gamma}_w$ is the wall shear rate. When instead the velocity across the layer is nearly uniform, $u \approx U$, the balance $U\,\partial_x T \sim a\,\partial_{yy} T$ gives

$$\delta_T \sim \left(\frac{a\,x}{U}\right)^{1/2}, \qquad \mathrm{Nu} \sim \left(\mathrm{Pe}\,\frac{d}{x}\right)^{1/2} = \left(\mathrm{Re}\,\mathrm{Pr}\,\frac{d}{x}\right)^{1/2}, \tag{94}$$

with $\mathrm{Pe} = U\,d/a$. The residence-time construction of Section 6.1.4 advects the fluid element at the bulk velocity $\tilde{u}_b$, not the wall shear, and therefore selects the uniform-advection branch (94), with exponent $1/2$ rather than $1/3$.

Branch (94) is exact for a constant-property fluid in uniform motion at velocity U under a constant wall flux q_w, with the thermal layer thin enough that the medium is semi-infinite in y. The Lagrangian substitution $t = x/U$ maps the steady balance onto one-dimensional transient conduction with constant surface flux,

$$\frac{\partial T}{\partial t} = a\,\frac{\partial^2 T}{\partial y^2}, \qquad -\lambda\,\frac{\partial T}{\partial y}\bigg|_{y=0} = q_w, \tag{95}$$

whose surface temperature is [47]

$$T_w(x) - T_\infty = \frac{2\,q_w}{\lambda}\sqrt{\frac{a\,x}{\pi\,U}}, \tag{96}$$

so that $\alpha = q_w/(T_w - T_\infty)$ yields

$$\mathrm{Nu}_x = \frac{\alpha\,d}{\lambda} = \frac{\sqrt{\pi}}{2}\left(\mathrm{Re}\,\mathrm{Pr}\,\frac{d}{x}\right)^{1/2}, \tag{97}$$

the plug penetration law.

The barrier regime follows by two substitutions: $U \to \tilde{u}_b$, and a by the diffusivity governing penetration across the barrier. The property peak damps, but does not extinguish, the turbulent momentum transport, so that $\varepsilon_{m,\mathrm{barrier}} \sim \nu$; with $\mathrm{Pr}_t = O(1)$ this implies $\varepsilon_{h,\mathrm{barrier}} \sim \nu$, consistent with the DNS evidence of turbulent heat-flux damping across the pseudocritical layer [45, 46]. The penetration of the front across the barrier is therefore governed by the barrier Péclet number

$$\mathrm{Pe}_t = \frac{\tilde{u}_b\,d}{\varepsilon_{h,\mathrm{barrier}}} \sim \frac{\tilde{u}_b\,d}{\nu} = \mathrm{Re}, \tag{98}$$

and

$$\mathrm{Nu} \sim \mathrm{Pe}_t^{1/2} \sim \sqrt{\mathrm{Re}}, \tag{99}$$

recovering Eqs. (71)–(73). No Prandtl factor accompanies the exponent: the penetration is set by the kinematic scale ν, not the thermal diffusivity $a = \nu/\mathrm{Pr}$, so (98) is a pure Reynolds number. The molecular-Prandtl dependence enters instead through the impedance integral of Section 3.2, as the factor $\mathrm{Pr}_b^{-1/2}(\mathrm{Pr}_b/\mathrm{Pr}_w)^{1/4}$ of the linearised form (84).

References

[1] A. Vasic, T. Beuthe, H. Zahlan, A. Nava-Dominguez, D. Wang, State of the art report on heat transfer at supercritical pressures, Canadian Nuclear Laboratories, Chalk River, ON, Canada (2023).

[2] I. L. Pioro, H. F. Khartabil, R. B. Duffey, Heat transfer to supercritical fluids flowing in channels—empirical correlations (survey), Nuclear Engineering and Design 230 (2004) 69–91. doi:10.1016/j.nucengdes.2003.10.010, foundational survey of HTD in supercritical fluids.

[3] J. Y. Yoo, The turbulent flows of supercritical fluids with heat transfer, Annual Review of Fluid Mechanics 45 (2013) 495–525. URL: https://www.annualreviews.org/content/journals/10.1146/annurev-fluid-120710-101234. doi:https://doi.org/10.1146/annurev-fluid-120710-101234.

[4] I. Pioro, R. Duffey, Heat Transfer and Hydraulic Resistance at Supercritical Pressures in Power Engineering Applications, ASME Press, New York, USA, 2007. 334 p.

[5] S. A. Wright, R. F. Radel, M. E. Vernon, G. E. Rochau, P. S. Pickard, Operation and Analysis of a Supercritical CO_2 Brayton Cycle, Technical Report SAND2010-0171, Sandia National Laboratories, 2010. URL: https://digital.library.unt.edu/ark:/67531/metadc1014473/, describes Sandia's sCO_2 cycle analysis tools, including CycleAnalysis for performance prediction, compressor operation near critical point, and loop design.

[6] J. Jackson, Fluid flow and convective heat transfer to fluids at supercritical pressure, Nuclear Engineering and Design 264 (2013) 24–40. URL: https://www.sciencedirect.com/science/article/pii/S0029549313000976. doi:https://doi.org/10.1016/j.nucengdes.2012.09.040, sI:NURETH-14.

[7] M. Pizzarelli, The status of the research on the heat transfer deterioration in supercritical fluids: A review, International Communications in Heat and Mass Transfer 95 (2018) 132–138. doi:10.1016/j.icheatmasstransfer.2018.05.001.

[8] A. Moisseytsev, J. J. Sienicki, PDC: Plant Dynamics Code for Design and Transient Analysis of Supercritical Brayton Cycles, Technical Report ANL-ART-154, Nuclear Science and Engineering Division, Argonne National Laboratory, 2018. URL: https://publications.anl.gov/anlpubs/2018/10/146715.pdf, system-level code for steady-state and transient simulation of sCO_2 Brayton cycles; widely used for nuclear-coupled and other sCO_2 power systems.

[9] RELAP5, Webpage, https://inl.gov/relap53d/, 2026. Last visited: 17.02.2026.

[10] APROS, Webpage, https://www.apros.fi/, 2026. Last visited: 16.02.2026.

[11] ECC-SMART, EU Grant Agreement ID: 945234, Project webpage, https://cordis.europa.eu/project/id/945234, 2020. Last visited: 02.04.2026.

[12] T. Schulenberg, I. Otić, Concept of a small modular SCWR with horizontal fuel assemblies, ASME Journal of Nuclear Engineering and Radiation Science 8 (2022) 031104. URL: https://doi.org/10.1115/1.4052191.

[13] I. Otić, Overview of the European supercritical-water-cooled small modular reactor concept, Thermal Science 30 (2026) 441–452. URL: https://doi.org/10.2298/TSCI25002440. doi:10.2298/TSCI25002440.

[14] I. Otić, T. Schulenberg, M. Šípová, A. Sáez-Maderuelo, S. Czifrus, L. Cizelj, European supercritical water-cooled small modular reactor: Design and analysis, Nuclear Engineering and Design 458 (2026) 115130. URL: https://www.sciencedirect.com/science/article/pii/S0029549326003821. doi:10.1016/j.nucengdes.2026.115130.

[15] A. Nava Dominguez, C. Azih, A. Mendoza España, H. Zahlan, G. Mazzini, A. Musa-Ruscak, S. Kassem, A. Pucciarelli, W. Ambrosini, F. Wiltschko, I. Otić, T. Varju, A. Kiss, P. Wu, E. Poplavskaia, A state-of-the-art review of r&d for the super critical water-cooled reactor technology. part i economics, thermalhydraulics, safety and licensing, Nuclear Engineering and Design 449 (2026) 114767. URL: https://www.sciencedirect.com/science/article/pii/S0029549326000191. doi:https://doi.org/10.1016/j.nucengdes.2026.114767.

[16] I. H. Bell, J. Wronski, S. Quoilin, V. Lemort, Pure and pseudo-pure fluid thermophysical property evaluation and the open-source thermophysical property library CoolProp, Industrial & Engineering Chemistry Research 53 (2014) 2498–2508. URL: https://doi.org/10.1021/ie4033999. doi:10.1021/ie4033999, the project website: http://www.coolprop.org.

[17] H. Swenson, J. Carver, C. Kakarala, Heat transfer to supercritical water in smooth-bore tubes, Trans. ASME, J. Heat Transfer, C 87 (1965) 477–484. doi:10.1115/1.3689139.

[18] V. Kurganov, Y. Zeigarnik, I. Maslakova, Heat transfer and hydraulic resistance of supercritical-pressure coolants. part i: Specifics of thermophysical properties of supercritical pressure fluids and turbulent heat transfer under heating conditions in round tubes (state of the art), International Journal of Heat and Mass Transfer 55 (2012) 3061–3075. doi:10.1016/j.ijheatmasstransfer.2012.01.031.

[19] V. Kurganov, Y. Zeigarnik, I. Maslakova, Heat transfer and hydraulic resistance of supercritical-pressure coolants. part ii: Experimental data on hydraulic resistance and averaged turbulent flow structure of supercritical pressure fluids during heating in round tubes under normal and deteriorated heat transfer conditions, International Journal of Heat and Mass Transfer 58 (2013) 152–167. doi:10.1016/j.ijheatmasstransfer.2012.11.044.

[20] V. Kurganov, Y. Zeigarnik, I. Maslakova, Heat transfer and hydraulic resistance of supercritical pressure coolants. part iii: Generalized description of scp fluids normal heat transfer, empirical calculating correlations, integral method of theoretical calculations, International Journal of Heat and Mass Transfer 67 (2013) 535–547. doi:10.1016/j.ijheatmasstransfer.2013.07.056.

[21] V. G. Razumovskiy, E. N. Pis'mennyi, K. Sidawi, I. L. Pioro, A. E. Koloskov, Experimental heat transfer in an annular channel and 3-rod bundle cooled with upward flow of supercritical water, Journal of Nuclear Engineering and Radiation Science 2 (2016) 011010. URL: https://doi.org/10.1115/1.4031818. doi:10.1115/1.4031818.

[22] International Atomic Energy Agency Technical Document, Understanding and prediction of thermohydraulic phenomena relevant to supercritical water cooled reactors (SCWRs), Technical Report IAEA-TECDOC-1900, International Atomic Energy Agency, Vienna, 2020. URL: https://www.iaea.org/publications/13636/understanding-and-prediction-of-thermohydraulic-phenomena-relevant-to-supercritical-water-c

[23] I. Otić, O. Ertunç, The thermal impedance integral and the pathway decomposition of supercritical turbulent heat transfer. Part II. Experimental validation and scope of the linearised pathway form, KITopen, preprint (2026). doi:10.5445/IR/1000196041.

[24] J. Jackson, W. Hall, Forced convection heat transfer to fluids at supercritical pressure, in: S. Kakač, D. Spalding (Eds.), Turbulent Forced Convection in Channels and Bundles, volume 2, Hemisphere, Washington, 1979, pp. 563–612.

[25] S. Rivkin, Thermophysical Properties of Water in Critical Region, Izd. Standartov, Moscow, 1970. P. 635 (in Russian).

[26] International Association for the Properties of Water and Steam, Revised Release on the IAPWS Industrial Formulation 1997 for the Thermodynamic Properties of Water and Steam, Technical Report, IAPWS, 2012. URL: https://www.iapws.org/public/documents/UWTF-/IF97-Rev.pdf.

[27] A. Bishop, R. Sandberg, L. Tong, Forced convection heat transfer to water at near-critical temperature and supercritical pressures, Technical Report WCAP-2056, Westinghouse Electric Corporation, Pittsburg, USA, 1964. (see also AICE, J. Chemical Engineering Symposium Series, No 2. London: Institute of Chemical Engineers, 1965).

[28] X. Zhao, W. Ambrosini, A. Pucciarelli, S. Kassem, T. Varju, A. Kiss, I. Otić, Y. Filonova, V. Filonov, Y. Zhu, B. Bi, Report on the results of the benchmark exercise, Technical Report Deliverable D3.2, ECC-SMART, 2023. URL: https://cordis.europa.eu/project/id/945234/.

[29] W. Ambrosini, I. Otić, T. Schulenberg, A. Pucciarelli, O. Chaaraoui, T. Varju, A. Kiss, B. Babcsány, C. Antók, P. Mészáros, Z. Bertesina, S. Czifrus, V. Filonov, D. Fedorov, Y. Filonova, Y. Dubyk, A. Nava-Dominguez, X. Zhao, Report on the preconceptual studies on the core layout and passive safety concept of the SCW-SMR, Technical Report Deliverable D3.3, ECC-SMART, 2024.

[30] T. Varju, A. Csige, A. Kiss, V. Filonov, Y. Filonova, D. Fedorov, A. Pucciarelli, S. Kassem, W. Ambrosini, Discussion and perspectives for improvements of heat transfer correlation capabilities for fluids at supercritical pressures, Nuclear Engineering and Design 421 (2024) 113085. URL: https://doi.org/10.1016/j.nucengdes.2024.113085. doi:10.1016/j.nucengdes.2024.113085.

[31] I. Otić, O. Ertunç, The Reynolds-number scaling of the Lyon integral and the structural rigidity of the Dittus–Boelter correlation, Preprint, KITopen, 2026.

[32] B. Petukhov, Heat transfer and friction in turbulent pipe flow with variable physical properties, volume 6 of *Advances in Heat Transfer*, Elsevier, 1970, pp. 503–564. URL: https://www.sciencedirect.com/science/article/pii/S0065271708701539. doi:https://doi.org/10.1016/S0065-2717(08)70153-9.

[33] R. N. Lyon, Liquid metal heat-transfer coefficients, Chemical Engineering Progress Symposium Series 47 (1951) 75–81.

[34] F. W. Dittus, L. M. K. Boelter, Heat Transfer in Automobile Radiators of the Tubular Type, Technical Report 13, University of California, Berkeley, Calif., 1930. Reprinted in International Communications in Heat and Mass Transfer, Vol. 12, pp. 3–22, 1985.

[35] V. V. Yakovlev, Local and mean heat-transfer for a turbulent flow of nonboiling water in a tube with high heat loads, The Soviet Journal of Atomic Energy 8 (1961) 221–224. URL: https://doi.org/10.1007/BF01481008. doi:10.1007/BF01481008.

[36] V. Gnielinski, Neue gleichungen für den wärme- und den stoffübergang in turbulent durchströmten rohren und kanälen, Forschung im Ingenieurwesen A 41 (1975) 8–16. URL: https://doi.org/10.1007/BF02559682. doi:10.1007/BF02559682.

[37] Z. Miropol'skii, M. Shitsman, Heat transfer to water and steam with variable specific heat, ZhTF (J. Tech. Phys.) 27 (1957) 2359–2372. (in Russian).

[38] E. Krasnoshchekov, V. Protopopov, Experimental studying of carbon dioxide heat transfer in supercritical region under high temperature differences, High Temperature 4 (1966) 389–398. (in Russian).

[39] A. Žukauskas, Heat transfer from tubes in crossflow, in: J. P. Hartnett, J. Irvine, Thomas F. (Eds.), Advances in Heat Transfer, volume 8, Academic Press, New York, 1972, pp. 93–160. URL: https://doi.org/10.1016/S0065-2717(08)70038-8. doi:10.1016/S0065-2717(08)70038-8.

[40] B. Petukhov, V. Kurganov, V. Ankudinov, Heat transfer and flow resistance in the turbulent pipe flow of a fluid with near-critical state parameters, High Temperature 21 (1983) 92–100. (in Russian).

[41] R. H. Kraichnan, Turbulent thermal convection at arbitrary prandtl number, The Physics of Fluids 5 (1962) 1374–1389. URL: https://doi.org/10.1063/1.1706533. doi:10.1063/1.1706533.

[42] X. Zhu, R. J. A. M. Stevens, O. Shishkina, R. Verzicco, D. Lohse, $Nu \sim Ra^{1/2}$ scaling enabled by multiscale wall roughness in Rayleigh–Bénard turbulence, Journal of Fluid Mechanics 869 (2019) R4. doi:10.1017/jfm.2019.228.

[43] S. Grossmann, D. Lohse, Scaling in thermal convection: a unifying theory, Journal of Fluid Mechanics 407 (2000) 27–56. doi:10.1017/S0022112099007545.

[44] G. Ahlers, S. Grossmann, D. Lohse, Heat transfer and large scale dynamics in turbulent Rayleigh-Bénard convection, Rev. Mod. Phys. 81 (2009) 503–537. doi:10.1103/RevModPhys.81.503.

[45] J. H. Bae, J. Y. Yoo, H. Choi, Direct numerical simulation of turbulent supercritical flows with heat transfer, Physics of Fluids 17 (2005) 105104. URL: https://doi.org/10.1063/1.2047588. doi:10.1063/1.2047588.

[46] Y. Bae, A new formulation of variable turbulent prandtl number for heat transfer to supercritical fluids, International Journal of Heat and Mass Transfer 92 (2016) 792–806. URL: https://www.sciencedirect.com/science/article/pii/S0017931015009771. doi:https://doi.org/10.1016/j.ijheatmasstransfer.2015.09.039.

[47] H. S. Carslaw, J. C. Jaeger, Conduction of Heat in Solids, 2 ed., Oxford University Press, Oxford, 1959.

[48] M. A. Lévêque, Les lois de la transmission de chaleur par convection, Annales des Mines, Mémoires, Série 12 13 (1928) 201–415.

[49] L. Graetz, Über die Wärmeleitungsfähigkeit von Flüssigkeiten, Annalen der Physik und Chemie 18 (1883) 79–94. Part 2: *ibid.* **25** (1885) 337–357.

[50] H. Schlichting, K. Gersten, Boundary-Layer Theory, 9 ed., Springer, Berlin, Heidelberg, 2017. URL: https://doi.org/10.1007/978-3-662-52919-5. doi:10.1007/978-3-662-52919-5.

[51] B. S. Petukhov, V. V. Kirillov, O teploperenose pri turbulentnom techenii zhidkosti v trubakh (about heat transfer in turbulent fluid flow in tubes), Teploenergetika (1958) 63–68. In Russian.

[52] E. N. Sieder, G. E. Tate, Heat transfer and pressure drop of liquids in tubes, Industrial & Engineering Chemistry 28 (1936) 1429–1435. URL: https://doi.org/10.1021/ie50324a027. doi:10.1021/ie50324a027.

[53] M. A. Mikheev, Osnovy teploperedachi, Gosenergoizdat, Moscow–Leningrad, 1956. In Russian.

[54] A. A. Žukauskas, Heat transfer of a single cylinder in crossflow, Teploenergetika No. 4 (1954) 38 ff. In Russian.

[55] P. P. Švenčianas, V. J. Makarevičius, M. M. Tamonis, A. A. Žukauskas, Heat transfer in tube banks in crossflow, Lietuvos TSR Mokslų Akademijos Darbai. Serija B 4(59) (1969) 149 ff. In Lithuanian.

[56] V. Protopopov, Generalizing dependences for local heat transfer coefficients during turbulent supercritical water and carbon dioxide flow in uniformly heated round tubes, High Temperature 15 (1977) 815–821. (in Russian).

[57] M. MacDonald, N. Hutchins, D. Chung, Roughness effects in turbulent forced convection, Journal of Fluid Mechanics 861 (2019) 138–162. doi:10.1017/jfm.2018.900.

[58] X. Zhu, R. J. A. M. Stevens, R. Verzicco, D. Lohse, Roughness-facilitated local 1/2 scaling does not imply the onset of the ultimate regime of thermal convection, Phys. Rev. Lett. 119 (2017) 154501. doi:10.1103/PhysRevLett.119.154501.

[59] D. Günseren, O. Ertunç, I. Ari, A. Atik, N. Muhtaroglu, I. Otić, Constructing a Reynolds stress model of decaying homogeneous isotropic turbulence using physics informed neural network, Journal of Computational Physics 553 (2026) 114725. URL: https://www.sciencedirect.com/science/article/pii/S0021999126000756. doi:https://doi.org/10.1016/j.jcp.2026.114725.